creative commons
COMMONS DEED

저작자표시-비영리-변경금지 2.0 대한민국

이용자는 아래의 조건을 따르는 경우에 한하여 자유롭게

- 이 저작물을 복제, 배포, 전송, 전시, 공연 및 방송할 수 있습니다.

다음과 같은 조건을 따라야 합니다:

저작자표시. 귀하는 원저작자를 표시하여야 합니다.

비영리. 귀하는 이 저작물을 영리 목적으로 이용할 수 없습니다.

변경금지. 귀하는 이 저작물을 개작, 변형 또는 가공할 수 없습니다.

- 귀하는, 이 저작물의 재이용이나 배포의 경우, 이 저작물에 적용된 이용허락조건을 명확하게 나타내어야 합니다.
- 저작권자로부터 별도의 허가를 받으면 이러한 조건들은 적용되지 않습니다.

저작권법에 따른 이용자의 권리는 위의 내용에 의하여 영향을 받지 않습니다.

이것은 이용허락규약(Legal Code)을 이해하기 쉽게 요약한 것입니다.

Disclaimer

dCollection

공학석사학위논문

Dynamic Increase Factor of Concrete Compressive Strength Considering the Pure Rate Effect

순수 변형속도 효과를 고려한 콘크리트 압축강도 동적증가계수

2017 년 8 월

서울대학교 대학원

건설환경공학부

이 상 호

ABSTRACT

Dynamic Increase Factor of Concrete Compressive Strength Considering the Pure Rate Effect

Lee, Sangho

Department of Civil & Environmental Engineering

The Graduate School

Seoul National University

Structures under extreme events like collision of car, ship, and aircraft, explosion, earthquake, tsunami, etc. are loaded at higher deformation rate than that under quasi-static state. Therefore, in order to design economically and analyze accurately concrete structures under extreme events, dynamic material properties of structures should be investigated.

Meanwhile, concrete is the material having the rate dependent property, which is that material properties like compressive and tensile strength, critical strain, etc. are changed along strain rate. Especially, concrete compressive strength becomes higher as strain rate is increased. It is caused by two reasons. First, loading duration of extreme events is too short to propagate cracks. Second, water in voids induces the inertia effects to resist deformation. This phenomenon is called the rate effect on concrete compressive strength, and dynamic increase factor (DIF) has been used widely to consider the rate effect in analysis and design of concrete structures.

Various DIFs have been suggested until now, but the DIFs have common problems. First of all, DIF has been assumed as a function of only strain rate, so other variables like static strength, strain acceleration, specimen shape, density, etc., which can influence on results of dynamic material test, were not considered. Therefore, the test data of DIF was spread widely at a strain rate point. Furthermore, the test data of DIF includes the axial and radial inertia effects, but the inertia effects were misinterpreted as the rate effect. However, the inertia effects are already covered in the equation of motion, so nonconservative results can be derived by considering repetitively the inertia effects in a constitutive equation with DIF.

In this study, analytical model of split Hopkinson pressure bar (SHPB) test for a linear elastic specimen was investigated to find out important variables causing the inertia effects in dynamic material test. Then, apparent DIF was suggested with the key factors by conducting nonlinear regression analysis for concrete SHPB test results. Finally, DIF considering the pure rate effect was suggested by correcting the inertia effects in apparent DIF. In order to verify proposed DIF, finite element analyses for concrete SHPB tests with proposed and representative DIFs were performed, and it was confirmed that proposed DIF predicts apparent dynamic strength of specimens with high accuracy.

Methodology correcting the inertia effects in results of dynamic material test in this study can be extended for evaluations of impact and explosion resistance performances of cementitious material like fiber reinforced concrete, etc. Furthermore, it is expected that the proposed DIF can be applied

to design, evaluation of safety, and behavior analysis for concrete structures under extreme events.

Keywords: dynamic increase factor, rate effect, inertia effect, strain rate, strain acceleration, split Hopkinson pressure bar, concrete compressive strength

Student Number: 2015-22930

TABLE OF CONTENTS

LIST OF TABLES

LIST OF FIGURES

NOTATIONS

Symbol		Definition and description
A_b	=	Area of bar components
A_s	=	Area of specimen
DIF	=	Dynamic increase factor
$DIF_{apparent}$	=	Apparent DIF
DIF_{rate}	=	DIF due to the pure rate effect
E_b	=	Young's modulus of bar components
E_k	=	Kinetic energy of specimen
E_p	=	Deformation energy of specimen
E_s	=	Young's modulus of specimen
$\dot{E}_k$	=	Temporal rate of kinetic energy of specimen
$\dot{E}_p$	=	Temporal rate of deformation energy of specimen
F	=	Force
T	=	Traction
W_{ext}	=	External work for specimen
$\dot{W}_{ext}$	=	Temporal rate of external work for specimen
$c_{1,b}$	=	Stress wave propagation speed of bar components
$c_{1,s}$	=	Stress wave propagation speed of specimen
d_s	=	Diameter of specimen

$\dot{d}_s$	=	Temporal rate of diameter of specimen
f_c'	=	Compressive strength of concrete
$f_{c,static}$	=	Static compressive strength of concrete
k_1	=	The first parameter in proposed apparent DIF
k_2	=	The second parameter in proposed apparent DIF
k_3	=	The third parameter in proposed apparent DIF
l_s	=	Length of specimen
$\dot{l}_s$	=	Temporal rate of length of specimen
m	=	Mass
s	=	Distance from reference to specimen
t	=	Time
u	=	Displacement of particle
v	=	Velocity of particle
v_1	=	Particle velocity of interface between specimen and incident bar
v_2	=	Particle velocity of interface between specimen and transmitted bar
v_d	=	Deformation velocity of specimen
v_{st}	=	Impact velocity of striker bar
$\dot{v}_1$	=	Temporal rate of particle velocity of interface between specimen and incident bar
$\dot{v}_2$	=	Temporal rate of particle velocity of interface between specimen and transmitted bar
$\dot{v}_d$	=	Temporal rate of deformation velocity of specimen

Δf_c	=	Total dynamic strength enhancement of specimen
$\Delta f_{inertia}$	=	Dynamic strength enhancement of specimen due to the axial and radial inertia effects
Δf_{rate}	=	Dynamic strength enhancement of specimen due to the rate effect
Π	=	Least square error function
β	=	Material parameter in formula of Mihashi and Wittmann (1980)
ε	=	Strain
ε_c	=	Strain of concrete
ε_i	=	Incident strain wave
ε_r	=	Reflected strain wave
ε_s	=	Axial strain of specimen
ε_t	=	Transmitted strain wave
$\dot{\varepsilon}$	=	Strain rate
$\dot{\varepsilon}_c$	=	Strain rate of concrete
$\dot{\varepsilon}_{c0}$	=	Reference strain rate of DIF in fib MC2010
$\dot{\varepsilon}_s$	=	Axial strain rate of specimen
$\dot{\varepsilon}_{s,static}$	=	Axial strain rate of specimen under quasi-static uniaxial compressive test
$\ddot{\varepsilon}_s$	=	Axial strain acceleration of specimen
ν_s	=	Poisson ratio of specimen
ρ_b	=	Density of bar components
ρ_s	=	Density of specimen

σ = Stress

σ_1 = Traction of interface between specimen and incident bar

σ_2 = Traction of interface between specimen and transmitted bar

σ_i = Incident stress wave

σ_r = Reflected stress wave

σ_s = Axial stress of specimen

σ_t = Transmitted stress wave

$\dot{\sigma}$ = Loading rate of concrete

$\dot{\sigma}_0$ = Reference loading rate of concrete

1. Introduction

1.1. Research Background

Recently, as design life of structures becomes longer, probability that structures suffer extreme events becomes higher. In other words, demand level of structures for loads becomes higher. In addition, terror has occurred consistently after the 9.11 terror, and the frequency of terror occurrence is also increased all over the world. For these reasons, demand for safety of structures from extreme events has been raised.

Because structures under extreme events like collision of car, ship, and aircraft, explosion, severe earthquake, tsunami, etc. are loaded at higher deformation rate than that under quasi-static state as shown in Figure 1.1, dynamic material properties should be investigated to design safely structures under extreme events and to evaluate safety of existing structures from extreme events.

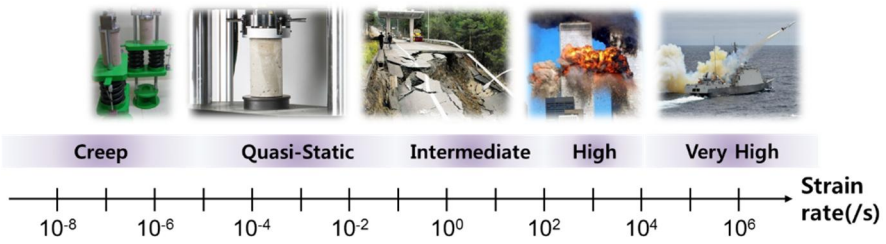

Figure 1.1 Strain rate in accordance with various events

Meanwhile, concrete is a rate dependent material, whose some material properties like compressive and tensile strength, critical strain, etc. are varied

sensitively along strain rate. Especially, concrete compressive strength becomes higher as strain rate is increased, and this phenomenon is described by two following causes (Li and Meng 2003).

1. Loading duration of extreme events is too short to propagate cracks.

2. Water in voids induces inertia effects to resist deformation.

This dynamic strength enhancement is called the rate effect on concrete compressive strength.

Dynamic increase factor (DIF) is broadly used to consider the rate effect in a constitutive equation. DIF is a factor multiplied by a static property. In general, DIF is defined by a ratio of a dynamic material property to a static material property such as Eq. 1.1. In a narrow sense, DIF is considered as compressive strength ratio such as Eq. 1.2. In this study, DIF of concrete compressive strength was only covered.

$$DIF = \frac{\left(\text{Dynamic material property}\right)}{\left(\text{Static material property}\right)} \tag{1.1}$$

$$DIF = \frac{\left(\text{Dynamic compressive strength}\right)}{\left(\text{Static compressive strength}\right)} \tag{1.2}$$

Various DIFs have been suggested by researchers, and there are representative DIFs in ACI 349-13 (Eq. 1.3), ACI 370R-14 (Eq. 1.4), fib MC2010 (Eq. 1.5), and UFC 3-340-02 (provided by graphs). Figure 1.2 shows the DIFs along strain rate in log scale.

$$DIF = \min\left[0.9 + 0.1\{\log_{10}\dot{\varepsilon}_c + 5\}, 1.25\right] \geq 1 \tag{1.3}$$

$$DIF = \begin{cases} 0.00965\log_{10}\dot{\varepsilon}_c + 1.058 \geq 1 & \text{for } \dot{\varepsilon}_c \leq 63.1 s^{-1} \\ 0.758\log_{10}\dot{\varepsilon}_c - 0.289 \leq 2.5 & \text{for } 63.1 s^{-1} < \dot{\varepsilon}_c \end{cases} \tag{1.4}$$

$$DIF = \begin{cases} \left(\dot{\varepsilon}_c / \dot{\varepsilon}_{c0}\right)^{0.014} & \text{for } 30\times10^{-6} s^{-1} \leq \dot{\varepsilon}_c \leq 30 s^{-1} \\ 0.012\left(\dot{\varepsilon}_c / \dot{\varepsilon}_{c0}\right)^{1/3} & \text{for } 30 s^{-1} < \dot{\varepsilon}_c \leq 300 s^{-1} \end{cases} \tag{1.5}$$

where, $\dot{\varepsilon}_{c0} = 30\times10^{-6} s^{-1}$

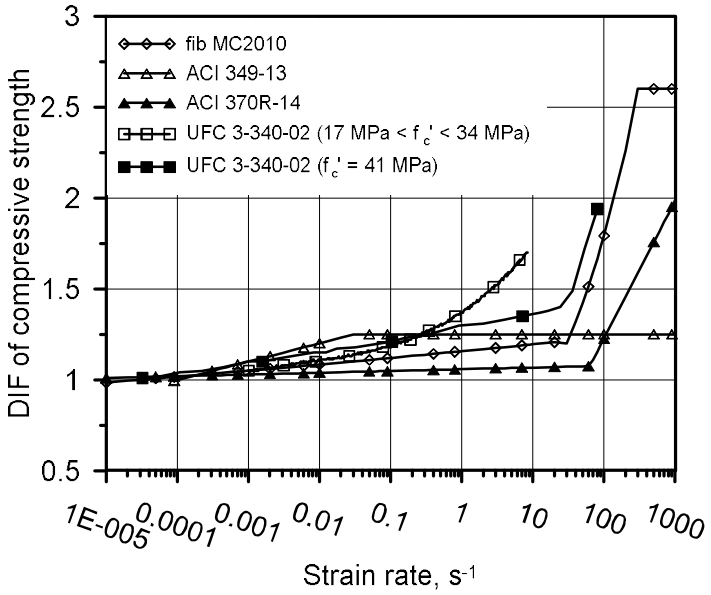

Figure 1.2 Various DIFs

However, these DIFs have three common problems. First, no one knows which DIF is realistic. Due to absence of standard dynamic material test method, researchers have carried out dynamic material tests with different method from one another, so the suggested DIFs are different from one

another as shown in Figure 1.2. Accordingly, analysis results with each DIF are different from one another as shown in Figure 1.3 which shows analyses results for concrete split Hopkinson pressure bar (SHPB) test. Brief explanation of SHPB test is described in chapter 2.1.

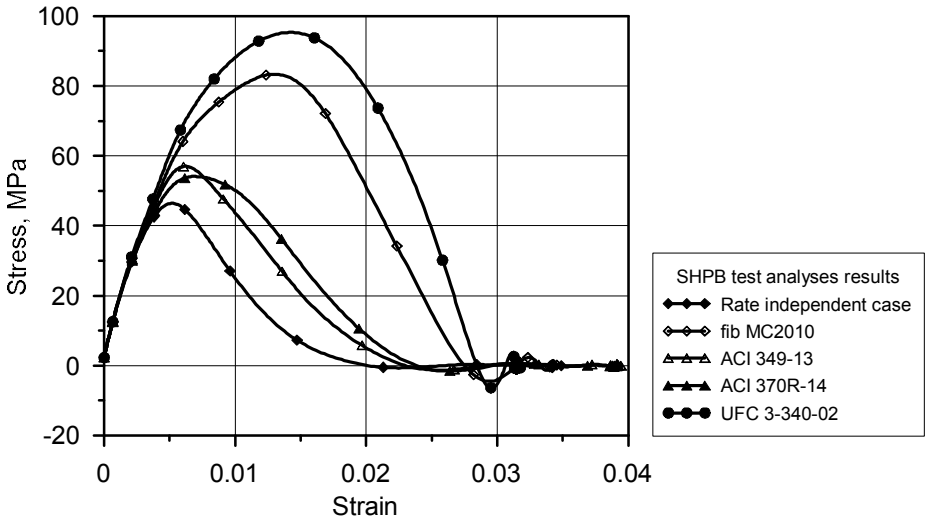

Figure 1.3 Analyses results of concrete SHPB test using various DIFs

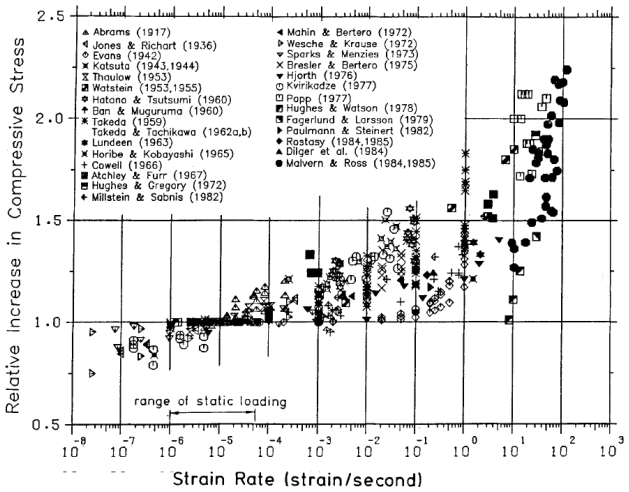

Figure 1.4 Test data of DIF (Bischoff and Perry 1991)

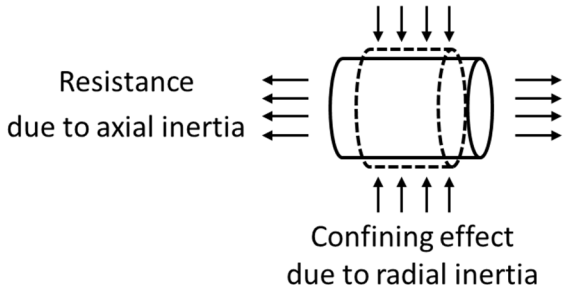

Figure 1.5 Inertia effects in dynamic material test

Second, the current DIFs have been assumed as a function of strain rate only. However, test data of DIF was spread widely at a strain rate point as shown in Figure 1.4 (Bischoff and Perry 1991). It means that other variables like static strength, strain acceleration, specimen shape and size, density, etc. can influence results of dynamic material test. Therefore, these variables should be considered to evaluate DIF.

Third, most importantly, the axial and radial inertia effects in dynamic material test cannot be avoidable because of nature of dynamic material test that it is impossible to control axial and radial deformation velocities of a specimen consistently as shown in Figure 1.5. However, the inertia effects are considered as the rate effect by misconception (Li and Meng 2003, Li et al. 2009, Zhang et al. 2009). Accordingly, some researchers have insisted that steep increase of dynamic strength result from the inertia effects rather than the rate effect (Bischoff and Perry 1991, Li and Meng 2003, Zhang et al. 2009, Kim et al. 2010, Magallanes et al. 2010, Hao et al. 2013), and DIF including the inertia effects as well as the rate effect has been called apparent DIF. If apparent DIF is applied to finite element analysis (FEA) of structures under

extreme events, the inertia effects are considered repeatedly at both equation of motion and a constitutive equation. As a result, apparent DIF leads to nonconservative results.

In this study, DIF due to pure rate effect was suggested to solve above mentioned problems by introducing important variables influencing the inertia effects in dynamic material test and by eliminating the inertia effects from apparent DIF. After that, numerical verification of proposed DIF was conducted to check its prediction accuracy.

1.2. Research Objectives and Scope

There are two main objectives in this study. One of main objectives of this study is finding out key factors inducing the inertia effects in dynamic material test of concrete, and evaluating apparent DIF separated into the rate effect and the inertia effects.

The other main objective is suggestion for DIF of concrete compressive strength due to the pure rate effect by eliminating the inertia effects from apparent DIF, and numerical verification of its prediction accuracy.

For these objectives, this study is divided by two main parts. The first main part is suggestion for DIF considering the pure rate effect. The first main part is divided by three minor parts. The first minor part is evaluation into analytical model of dynamic material test for a linear elastic specimen to find out important variables inducing the axial and radial inertia effects. The second minor part is concrete SHPB test procedure and its results to obtain test data of apparent DIF for regression analysis. The last minor part is nonlinear regression analysis to propose DIF considering the pure rate effect. The other main part is verification of proposed DIF. For this, the second main part consists of two minor parts, which are verification analyses and its results respectively.

1.3. Outline

Chapter 1 indicates the introduction such as the background, objectives, scope, and outline of this study.

Chapter 2 presents basic concept of SHPB test and literature reviews of previous studies. Furthermore, limitations of the previous studies were described.

Chapter 3 includes investigation into analytical model of SHPB test to figure out important variables to influence the inertia effects in dynamic material test. In addition, SHPB test procedure and its results for regression analysis are presented. Finally, by conducting nonlinear regression analysis, DIF considering the pure rate effect was suggested.

Verification analyses were conducted to check prediction accuracy of proposed DIF in chapter 4, and comparison with other DIFs is also presented.

Finally, conclusions of this study are summarized in chapter 5.

2. Theoretical Background

Split Hopkinson pressure bar (SHPB) test has been widely used to evaluate dynamic material properties of metal, ceramic, rock, polymer, concrete, etc. In this study, SHPB was used to obtain dynamic strength of concrete, and also in previous studies, numerical, experimental, and analytical studies for SHPB test were performed to investigate dynamic material properties of concrete and the inertia effects on dynamic strength. Therefore, basic concept of SHPB test was briefly described firstly. Then, significances and limitations of previous studies were presented.

2.1. Split Hopkinson Pressure Bar Test

2.1.1. Principle of SHPB test

SHPB was developed by H. Kolsky in 1949 (Gray et al. 2000), and has been widely used to evaluate dynamic stress-strain relation of metal, ceramic, rock, polymer, concrete, etc. at intermediate and high strain rate region. SHPB consists of a striker bar, an incident bar, a transmitted bar, and measurement system such as strain gauges on the surfaces of the bar components as shown in Figure 2.1. In general, the bar components are made with the same material and the same cross-section as one another. v_1, v_2, and v_{st} mean particle velocities of interfaces between specimen and the bar components, and impact velocity of striker bar respectively.

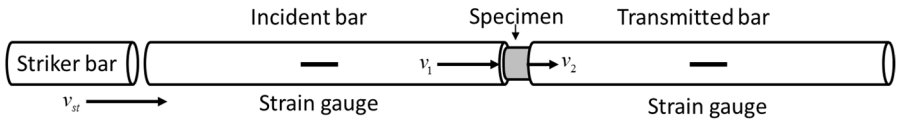

Figure 2.1 Components of SHPB

Principle of SHPB is based on one-dimensional stress wave theory, and that means any distortional stress wave is not generated in the bar components. In addition, the bar components remain linear elastic. In this case, the governing equation of the bar components is expressed as Eq. 2.1, and the relations between particle velocity and stress, and between particle velocity and strain are expressed as Eq. 2.2 and 2.3 from elementary wave theory. $c_{1,b}$, u_x, v_x, ε_x, ρ_b, and σ_x mean wave propagation velocity of the bar components, displacement of particle in the axis direction, particle velocity in the axis direction, strain of the bar components in the axis direction, density of the bar components, and stress of the bar components in the axis direction respectively.

$$\frac{\partial^2 u_x}{\partial t^2} - c_{1,b}{}^2 \frac{\partial^2 u_x}{\partial x^2} = 0 \tag{2.1}$$

$$\sigma_x = \rho_b c_{1,b} v_x \tag{2.2}$$

$$v_x = c_{1,b} \varepsilon_x \tag{2.3}$$

When the striker bar impacts the incident bar, an incident stress wave propagates through the incident bar. And then, when the incident stress wave arrives on the interface between a specimen and the incident bar, a part of the

incident stress wave, which is a reflected stress wave, is reflected and returns through the incident bar, and the other part of the incident stress wave, which is a transmitted stress wave, is transmitted to the specimen and the transmitted bar due to lower impedance of the specimen than that of the bar components. At this moment, these stress waves disturb particles of the bar components, and the particles are vibrated as shown in Eq. 2.2 and 2.3. As a result, particles on interfaces between the specimen and the bar components are moved as shown in Figure 2.2, so the specimen is compressed due to the relative velocity between both specimen ends.

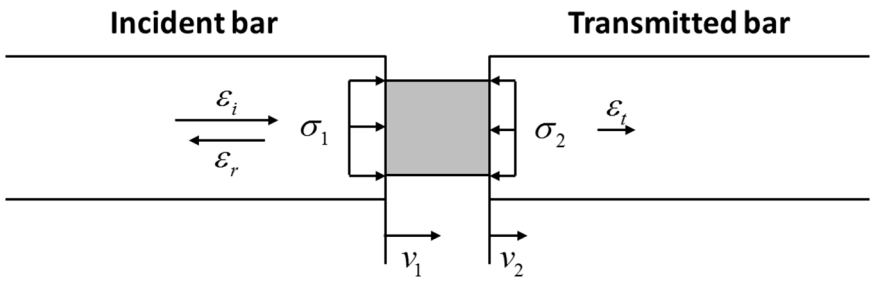

Figure 2.2 Strain waves, particle velocities and tractions on the specimen ends

From the Eq. 2.3, the particle velocities on the specimen ends can be expressed with strain waves as Eq. 2.4 and 2.5. The incident strain wave, the reflected strain wave, and the transmitted strain wave are measured by strain gauges on the surfaces of each bar separately, and these waves are shifted to the time when the incident wave arrives on the interface between the incident bar and the specimen. Sign of compression is taken as positive.

$$v_1 = c_{1,b}\left(\varepsilon_i - \varepsilon_r\right) \tag{2.4}$$

$$v_2 = c_{1,b}\varepsilon_t \tag{2.5}$$

Meanwhile, average strain rate of the specimen can be obtained by Eq. 2.6. By substituting Eq. 2.4 and 2.5 to Eq. 2.6, strain rate can be expressed by Eq. 2.7. Then, engineering strain of the specimen can be calculated by integrating Eq. 2.7 such as Eq. 2.8.

$$\dot{\varepsilon}_s = \frac{v_1 - v_2}{l_s} \tag{2.6}$$

$$\dot{\varepsilon}_s = c_{1,b}\left(\frac{\varepsilon_i - \varepsilon_r - \varepsilon_t}{l_s}\right) \tag{2.7}$$

$$\varepsilon_s = \int_0^t c_{1,b}\left(\frac{\varepsilon_i - \varepsilon_r - \varepsilon_t}{l_s}\right)d\tau \tag{2.8}$$

Traction conditions on the specimen ends can be obtained from Newton's 3rd law as Eq. 2.9 and 2.10 as shown in Figure 2.2. With the assumption of uniform stress and strain distribution in the specimen along the axial direction, stress of the specimen is expressed by average of the tractions such as Eq. 2.11.

$$\sigma_1 = \frac{A_b}{A_s}\left(\sigma_i + \sigma_r\right) \tag{2.9}$$

$$\sigma_2 = \frac{A_b}{A_s}\sigma_t \tag{2.10}$$

$$\sigma_s = \frac{A_b}{2A_s}\left(\sigma_i + \sigma_r + \sigma_t\right) \tag{2.11}$$

If dynamic equilibrium state is achieved in the specimen, the tractions should be same as each other. In this case, Eq. 2.12 is valid, so strain rate, strain, and stress of the specimen are expressed as Eq. 2.13, 2.14, and 2.15. By matching stress to strain in accordance with time, dynamic stress-strain relation of specimen can be obtained.

$$\sigma_i + \sigma_r = \sigma_t \tag{2.12}$$

$$\dot{\varepsilon}_s = \frac{2c_{1,b}\varepsilon_r}{l_s} \tag{2.13}$$

$$\varepsilon_s = \int_0^t \frac{2c_{1,b}\varepsilon_r}{l_s} d\tau \tag{2.14}$$

$$\sigma_s = \frac{A_b}{A_s}\sigma_t \tag{2.15}$$

2.1.2. Pulse shaped SHPB test

Because an incident wave rises very steeply in classic SHPB test like Figure 2.3, concrete specimen is not appropriate to classic SHPB test for two reasons. First, concrete specimen should be much larger than homogeneous specimen for representability. Furthermore, stress wave propagation velocity of concrete is lower than those of other materials. As a result, transferring stress wave toward the both ends of specimen is delayed as shown in Figure 2.4, so dynamic equilibrium cannot be achieved like Figure 2.5 and premature

failure can occur. Second, due to large diameter of concrete specimen, diameter of bar components should become large. In this case, the radial dilatation effect of bar components becomes stronger, so high frequency noise is more generated due to wave dispersion which violates the one-dimensional stress wave assumption (Lok et al. 2002). In order to solve these problem, pulse shaped SHPB technique is widely used for brittle materials like concrete.

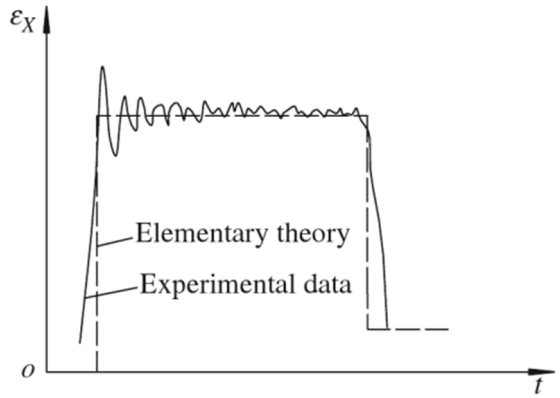

Figure 2.3 Typical incident strain wave in classic SHPB test (Wang 2007)

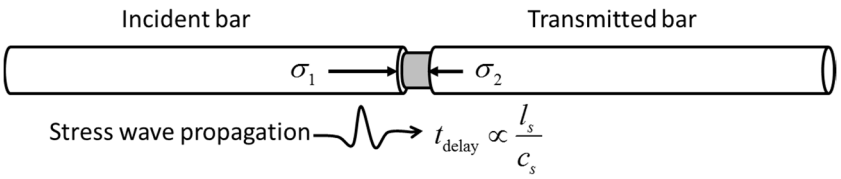

Figure 2.4 Delay of stress wave propagation in a specimen

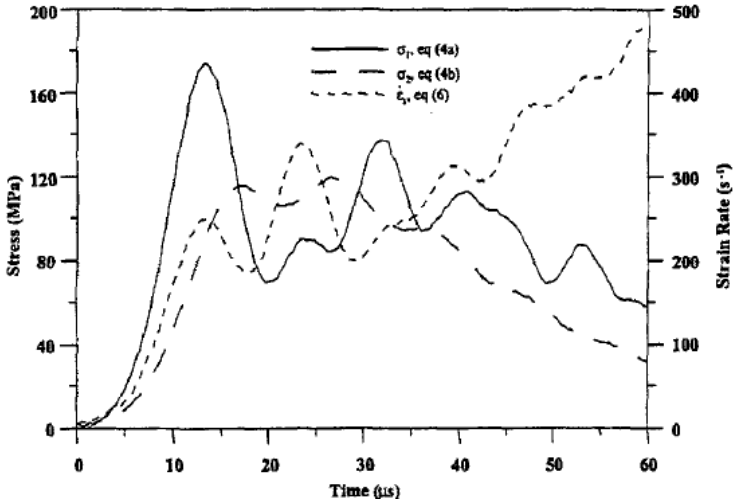

Figure 2.5 Dynamic non-equilibrium of limestone specimen from classic SHPB test (Frew et al. 2001)

Pulse shaper is used to make an incident wave slowly rise. Pulse shaper is attached on the impact face of an incident bar with a lubricant like Figure 2.6, and a striker bar impacts on pulse shaper. Then, an incident wave is slowly generated by reflection and transmission through pulse shaper. Figure 2.7 shows incident waves from SHPB test with and without pulse shaper. Accordingly, unbalance between tractions on both specimen ends is relieved, so dynamic equilibrium can be achieved in the specimen. Therefore, this study is focused on pulse shaped SHPB test.

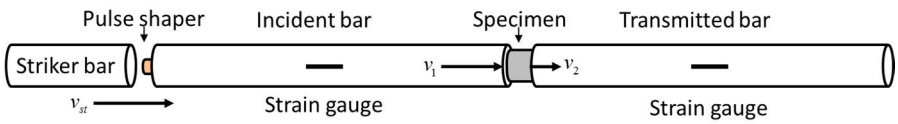

Figure 2.6 Configuration of pulse shaped SHPB test

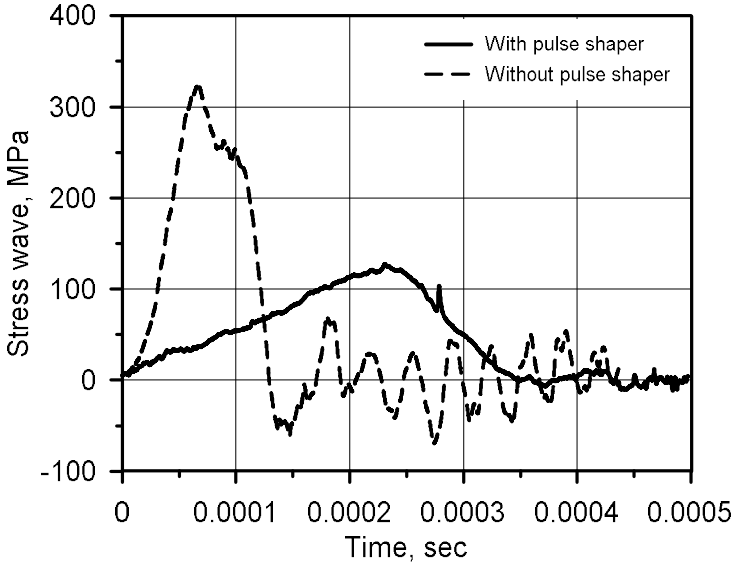

Figure 2.7 Comparison between incident waves with and without pulse shaper

2.2. Previous Studies

2.2.1. Apparent DIF

The change of the tendency in DIF cannot be explained with the rate effect (Li and Meng 2003). Therefore, some researchers tried to explain this phenomenon by other effects. Bischoff and Perry (1991) suggested that the steep increase of dynamic strength may result from a change in the deformation state from uniaxial stress to uniaxial strain by the confining effect due to the radial inertia effect and specimen ends friction rather than the rate effect as shown in Figure 2.8. In other words, the steep increase of DIF is not real material property but just structural effect. After Bischoff and Perry (1991), many researchers evaluated the apparent DIF, which includes the rate effect and other effects such as the ends friction and the inertia effects.

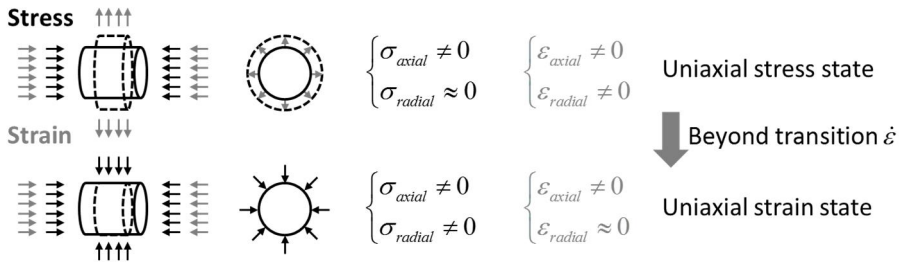

Figure 2.8 Change in the deformation state

2.2.2. Numerical studies

2.2.2.1 Li and Meng (2003)

Li and Meng (2003) conducted numerical study for concrete SHPB tests of Grote et al. (2001) with Drucker-Prager model, which is a pressure-dependent model. As a result, it was confirmed that the confining effect due to the radial inertia effect occurs as shown in Figure 2.9.

Furthermore, parameter study for various friction coefficients was conducted, so it was confirmed that friction can influence apparent DIF, but if friction coefficient is smaller than 0.1, the effect of friction can be neglected as shown in Figure 2.10. Therefore, the friction effect can be removed by lubricating the specimen ends.

However, the axial inertia effect was not considered, and a correction method to the inertia effects was not presented.

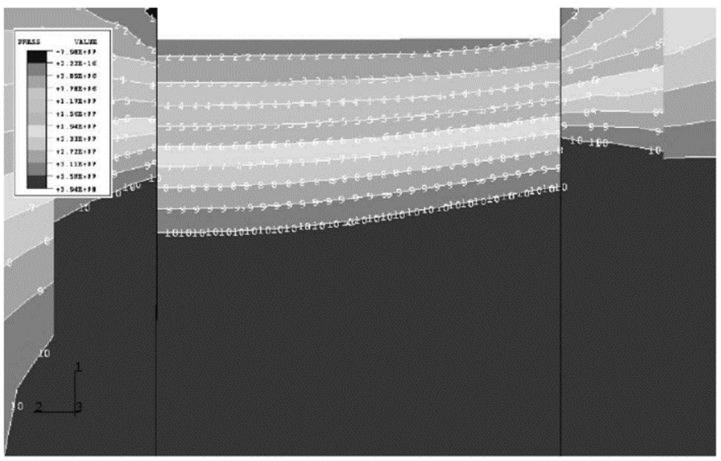

Figure 2.9 Contour of the hydrostatic stress in a specimen (Li and Meng 2003)

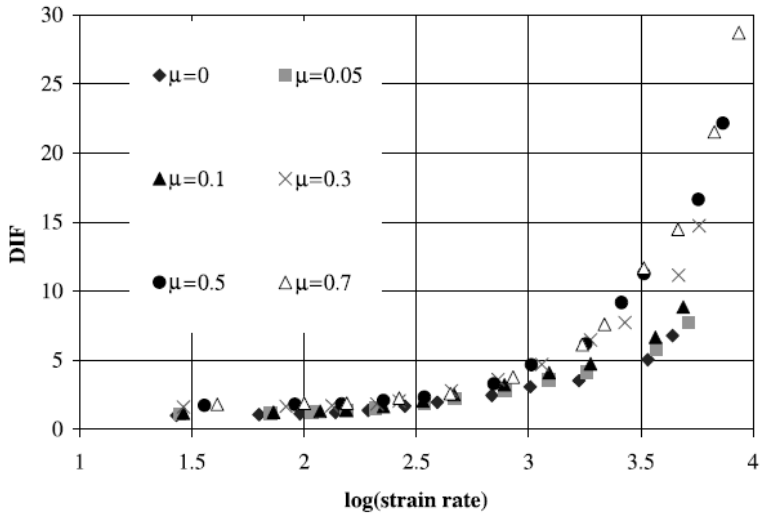

Figure 2.10 Results of parameter study for friction (Li and Meng 2003)

2.2.2.2 Kim et al. (2010)

Kim et al. (2010) conducted numerical analyses of concrete SHPB test of Ross et al. (1989, 1996) and Grote et al. (2001). Two rate independent models were used as material models. One is J_2 model, which is a pressure-independent model, and the other is modified Drucker-Prager model, which is a pressure-dependent model.

Because the models are rate independent, the dynamic enhancement in Figure 2.11 and 2.12 is not caused by the rate effect. In addition, because the difference between J_2 model and modified Drucker-Prager model is whether hydrostatic stress dependency is considered or not, and the results from modified Drucker-Prager model predicted the experimental data well as shown in Figure 2.11 and 2.12, Kim et al. (2010) insisted that the rate effect is

not dominant, but that the confining effect due to the radial inertia effect is dominant for the dynamic strength enhancement.

However, the number of analysis cases was small, and a part of analyses could not predict the experimental data, so it is difficult to say that the rate effect can be always neglected.

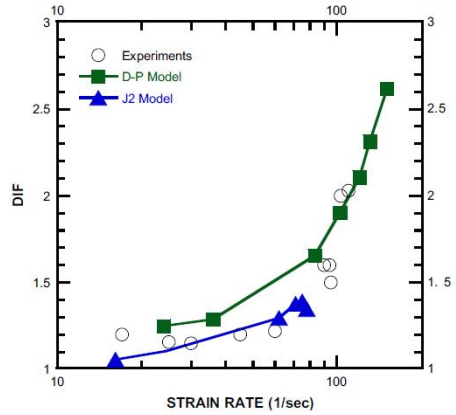

Figure 2.11 DIF versus strain rate for Ross's setup (Kim et al. 2010)

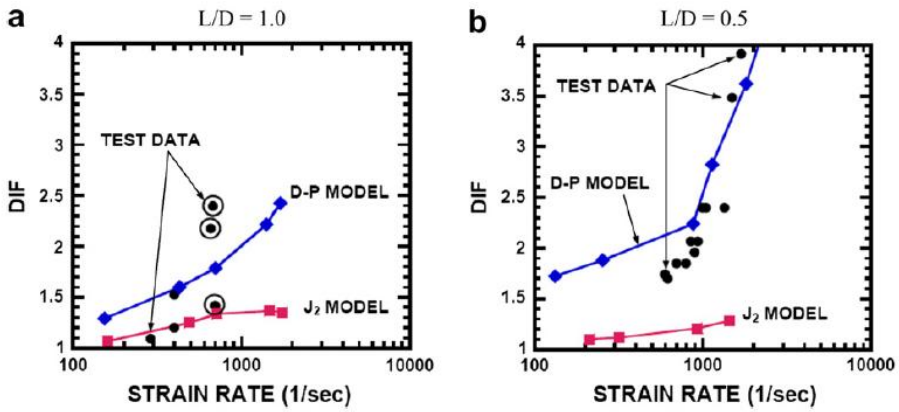

Figure 2.12 DIF versus strain rate for Grote's setup (Kim et al. 2010)

2.2.2.3 Magallanes et al. (2010)

Magallanes et al. (2010) conducted numerical analyses for concrete SHPB tests by applying concrete damage model, which is a pressure-dependent model, with various DIFs. Three DIFs, which were rate independency, DIF of CEB-FIP MC 1990, and DIF of CEB-FIP MC 1990 without steep increase respectively, were used as shown in Figure 2.13. As shown in Figure 2.14, the results indicated that the first case underestimated the dynamic strength, so it was insisted that the rate effect exists. Furthermore, the second case overestimated the dynamic strength, so it was confirmed that DIF of CEB-FIP MC 1990 includes the inertia effects as well as the rate effect. Finally, the third case predicted the dynamic strength well. Therefore, it was insisted that the steep increase of DIF is not real rate effect and is due to the inertia effects.

However, the simple extension of DIF curve within a transition strain rate is not reasonable because there was not any verification or any review.

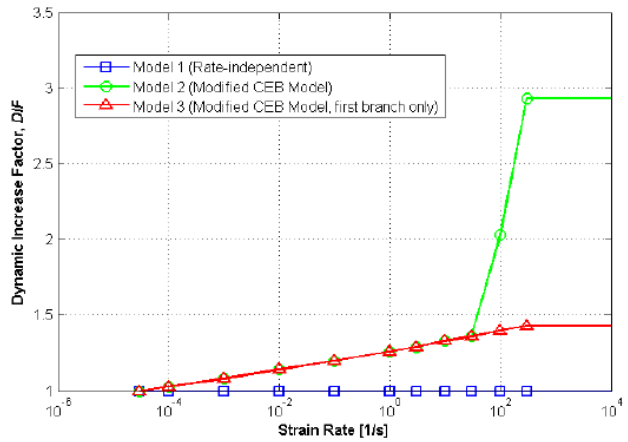

Figure 2.13 DIFs used in analyses (Magallanes et al. 2010)

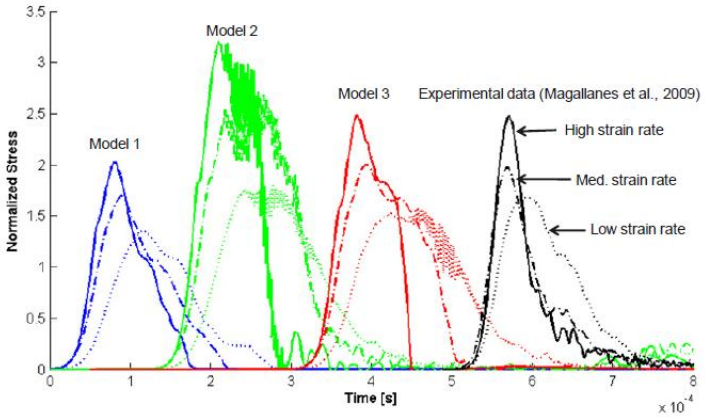

Figure 2.14 Results of analyses and SHPB test (Magallanes et al. 2010)

2.2.3. Experimental studies

2.2.3.1 Zhang et al. (2009)

Zhang et al. (2009) conducted SHPB tests for mortar specimens with various outer and inner diameters as shown in Figure 2.15, so confirmed experimentally that the radial inertia effect exists. For solid specimens, the confining effect due to the radial inertia effect at the center of a specimen is largest, and at the free surface is zero. Therefore, the larger outer diameter of specimen is, the larger the radial inertia effect is. Likewise, the smaller inner diameter of specimen is, the lager the radial inertia effect is for annular specimens. In other words, the dynamic strength enhancement becomes large for specimens with large outer diameter and small inner hole as shown in Figure 2.16.

However, the radial inertia effect cannot be completely eliminated by this test technique. Furthermore, if inner diameter becomes larger, loss of volume becomes bigger, so representability of a specimen becomes lower.

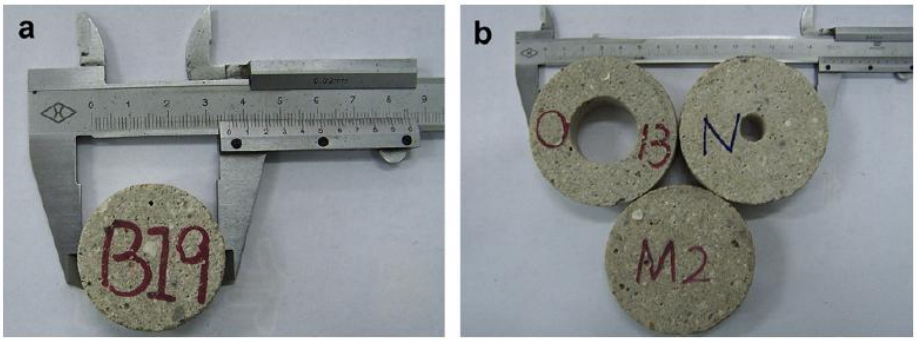

Figure 2.15 Mortar specimens for SHPB tests (Zhang et al. 2009)

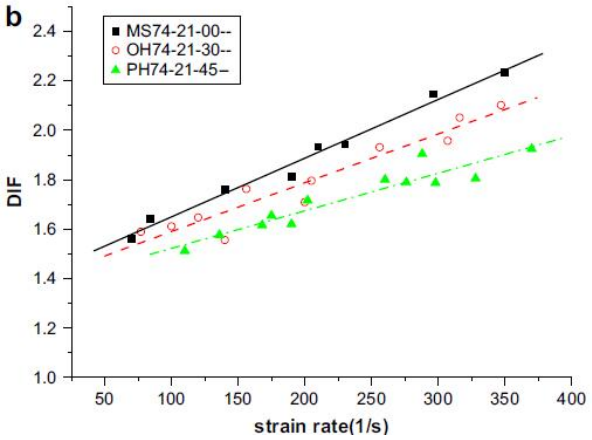

Figure 2.16 SHPB tests results for solid specimens and annular specimens with 30 mm and 45 mm inner hole (Zhang et al. 2009)

2.2.3.2 Hao et al. (2013)

Hao et al. (2013) conducted SHPB tests for mortar and concrete specimens with various diameter, and confirmed that the radial inertia effect

in SHPB test exists in the similar way to Zhang et al. (2009). The test results indicated that the dynamic strength becomes higher as diameter of specimen becomes lager, which means the lager radial inertia effect as show in Figure 2.17.

However, the axial inertia effect was not considered, and any correction method to the inertia effects or DIF considering the pure rate effect was not presented like as Li and Meng (2003).

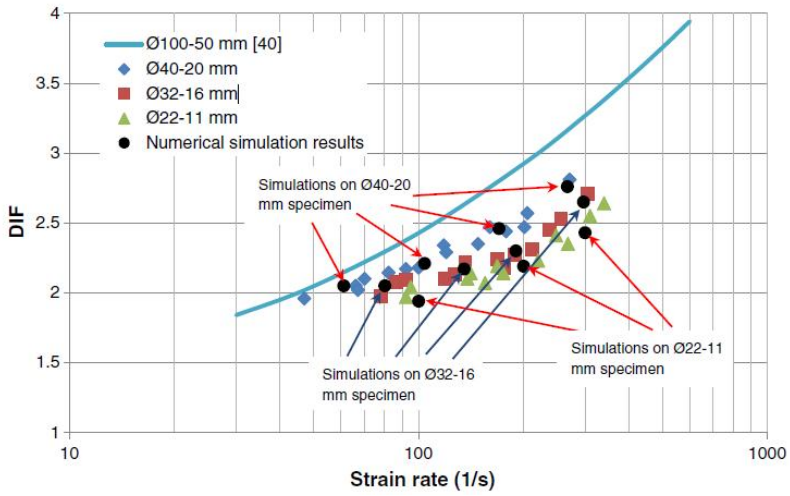

Figure 2.17 SHPB test results for various diameter specimens (Hao et al. 2013)

2.2.4. Analytical studies

2.2.4.1 Davies and Hunter (1963)

To investigate dynamic behaviors of metal and polymer specimens, Davies and Hunter (1963) evaluated the axial and radial inertia effects in SHPB test by solving energy balance equation. The axial and radial inertia effects were considered by particle velocities in the axial and radial directions

respectively in energy balance equation. The inertia effects were expressed as Eq. 2.16, which means that strain acceleration, dimension, and density of a specimen are important variables inducing the inertia effects in dynamic material test. Therefore, it was insisted that the inertia effects can be removed by manufacturing a specimen with L/D ratio of Eq. 2.17. d_s, l_s, $\Delta\sigma_{inertia}$, ε_s, ν_s, and ρ_s denote diameter, length, the inertia effects, strain, Poisson ratio and density of a specimen.

$$\Delta\sigma_{inertia} = \rho_s \left(\frac{l_s^2}{6} - \frac{\nu_s d_s^2}{8} \right) \ddot{\varepsilon}_s \tag{2.16}$$

$$\frac{l_s}{d_s} = \sqrt{\frac{3\nu_s}{4}} \approx 0.4 - 0.5 \tag{2.17}$$

However, Davies and Hunter (1963) omitted some inertia effect terms during approximation procedure (Samanta, 1971, Gorham 1989).

2.2.4.2 Gorham (1989)

Gorham (1989), in the similar way to Davies and Hunter (1963), the energy balancing equation was solved for the model of SHPB test for incompressible and perfectly plastic metal, so the inertia effects were obtained as Eq. 2.18. Gorham (1989) found out that square of strain rate influences also the inertia effects.

$$\Delta\sigma_{inertia} = \rho_s \left(\frac{l_s^2}{6} + \frac{d_s^2}{64} \right) \dot{\varepsilon}^2 + \rho_s \left(\frac{l_s^2}{6} - \frac{d_s^2}{32} \right) \ddot{\varepsilon}_s \tag{2.18}$$

However, it is not appropriate to concrete because yielding metal specimen was assumed.

2.2.4.3 Forrestal et al. (2007)

Forrestal et al. (2007) evaluated the radial inertia effect in SHPB test of a linear elastic specimen by solving equation of motion, stress-strain relations, and strain-displacement relations. Then, the radial inertia effects in the axial, radial, and tangential directions were expressed by closed form such as Eq. 2.19, 2.20, and 2.21. The results indicated also that strain acceleration, dimension, and density of a specimen are the key factors.

$$\Delta\sigma_{z,inertia}(r,t)=\frac{\nu_s^{\,2}(3-2\nu_s)}{4(1-\nu_s)}\left(\frac{d_s^{\,2}}{4}-\frac{2r^2}{(3-2\nu_s)}\right)\rho_s\ddot{\varepsilon}_s(t) \qquad (2.19)$$

$$\Delta\sigma_{r,inertia}(r,t)=\frac{\nu_s(3-2\nu_s)}{8(1-\nu_s)}\left(\frac{d_s^{\,2}}{4}-r^2\right)\rho_s\ddot{\varepsilon}_s(t) \qquad (2.20)$$

$$\Delta\sigma_{\theta,inertia}(r,t)=\frac{\nu_s(3-2\nu_s)}{8(1-\nu_s)}\left(\frac{d_s^{\,2}}{4}-\frac{(1+2\nu_s)r^2}{(3-2\nu_s)}\right)\rho_s\ddot{\varepsilon}_s(t) \qquad (2.21)$$

However, the rate effect, the axial inertia effect, and the hydrostatic stress dependent effect were not considered. Therefore, it is difficult to apply to concrete directly.

2.2.5. Summary and limitations of previous studies

Numerical, experimental, and analytical studies for SHPB tests have been carried out. As a result, it was theoretically and experimentally

confirmed that not only the rate effect but also the resistance due to the axial inertia effect and the confining effect due to the radial inertia effect and friction influence dynamic strength enhancement of concrete, so apparent DIF leads on nonconservative results in analysis and design of concrete structures. However, between two causes of the confining effect, friction can be easily removed by applying a lubricant to the specimen ends. Therefore, the main concern of this study was the axial and radial inertia effects in apparent DIF.

Because numerical and experimental studies were focused on only checking the existence of the inertia effects in SHPB tests, any correction method of the inertia effects in apparent DIF or DIF considering the pure rate effect was not presented. Furthermore, although, from analytical studies, it was found out that strain rate, strain acceleration, dimension, and density of a specimen are important variables inducing the inertia effects, the results of analytical studies cannot be applied to concrete SHPB test directly due to assumptions and omissions of the studies.

In order to overcome above mentioned limitations, evaluation of the inertia effects in concrete SHPB tests is needed. In this study, the analytical model of SHPB test for a linear elastic material was evaluated firstly. Then, a regression equation for apparent DIF was formulated with important variables determined from evaluation of the analytical model. Furthermore, concrete SHPB tests were conducted to obtain test data for regression analysis, and regression analysis was carried out using the data. Finally, DIF considering the pure rate effect was suggested by excluding the inertia effects from apparent DIF.

3. Suggestion of DIF Considering Pure Rate Effect

This chapter tried to overcome the limitations of previous studies as mentioned in chapter 2. First of all, analytical model of SHPB test was evaluated to determine a regression equation of apparent DIF. Furthermore, concrete SHPB test procedure and its results were presented for regression analysis. Finally, regression analysis was carried out to suggest apparent DIF separated into the rate effect and the inertia effects, and DIF due to the pure rate effect was suggested.

3.1. Important Variables Influencing Apparent DIF

3.1.1. Analytical model of SHPB test

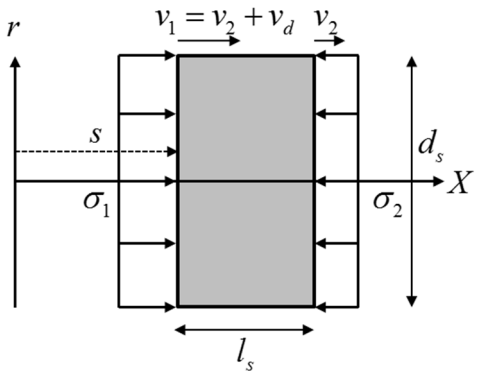

Figure 3.1 Analytical model of SHPB test for a linear elastic specimen

In order to figure out which variables influence the axial and radial inertia effects in dynamic material test, analytical model of SHPB test for a linear elastic specimen was investigated, and the inertia effects in SHPB test were obtained by solving energy balance equation. Figure 3.1 shows the

model. s, and v_d denote distance from reference to a specimen, and deformation velocity of specimen respectively. The other is same as earlier notation.

The followings were assumed in this model.

1. Axis-symmetric state
2. Uniform axial deformation
3. Linear stress-strain relationship
4. Rate independent property
5. Hydrostatic stress independent property
6. Constant Poisson ratio

From the assumption 1 and 2, particle velocities are expressed by Eq. 3.1 and 3.2. Sign of compressive strain and strain rate was taken as positive.

$$v_x(X) = v_2 + v_d - v_d \frac{X - s}{l_s} \tag{3.1}$$

$$v_r(r) = -\nu_s \dot{\varepsilon}_x r = -\nu_s \frac{v_d}{l_s} r \tag{3.2}$$

And then, the kinetic energy of the specimen, Eq. 3.3, is expressed as Eq. 3.4 by substituting Eq. 3.1 and 3.2 to Eq. 3.3.

$$E_k = \frac{1}{2}\rho_s \int_V \left(v_x^{\,2} + v_r^{\,2} \right) dV \tag{3.3}$$

$$E_k = \pi \rho_s d_s^{\,2} \left(\frac{1}{8} v_2^{\,2} l_s + \frac{1}{24} v_d^{\,2} l_s + \frac{1}{8} v_2 v_d l_s + \frac{v_s^{\,2}}{64} \frac{v_d^{\,2} d_s^{\,2}}{l_s} \right) \tag{3.4}$$

By differentiating Eq. 3.4 with respect to time, the temporal rate of the kinetic energy can be obtained as Eq. 3.5.

$$\dot{E}_k = \pi \rho_s d_s^{\,2} \left[\frac{\dot{d}_s}{d_s} \left(\frac{v_2^{\,2} l_s}{4} + \frac{v_d^{\,2} l_s}{12} + \frac{v_2 v_d l_s}{4} + \frac{v_s^{\,2}}{32} \frac{v_d^{\,2} d_s^{\,2}}{l_s} \right) + \left(\frac{v_2 \dot{v}_2 l_s}{4} + \frac{v_d^{\,3}}{24} + \frac{v_2^{\,2} v_d}{8} \right.\right.$$
$$\left.\left. + \frac{v_d \dot{v}_d l_s}{12} + \frac{v_2 \dot{v}_d l_s}{8} + \frac{\dot{v}_2 v_d l_s}{8} + \frac{v_2 v_d^{\,2}}{8} + \frac{v_s^{\,2}}{32} \frac{v_d \dot{v}_d d_s^{\,2}}{l_s} + \frac{v_s^{\,2}}{32} \frac{v_d^{\,2} d_s \dot{d}_s}{l_s} - \frac{v_s^{\,2}}{64} \frac{v_d^{\,3} d_s^{\,2}}{l_s^{\,2}} \right) \right] \tag{3.5}$$

Meanwhile, the deformation energy in the specimen is expressed by Eq. 3.6, and by differentiating Eq. 3.6 with respect to time with the assumption 1, 2, 3, and 4, the temporal rate of the deformation energy is expressed by Eq. 3.7.

$$E_p = \frac{1}{2} \int_V \sigma_{ij} \varepsilon_{ij} dV \tag{3.6}$$

$$\dot{E}_p = \frac{\pi d_s^{\,2}}{4} v_d E_s \varepsilon_x \tag{3.7}$$

From the traction boundary conditions, the temporal rate of external work for the specimen is expressed by Eq. 3.8.

$$\dot{W}_{ext} = \frac{\pi d_s^{\,2}}{4} \left\{ \sigma_1 \left(v_d + v_2 \right) - \sigma_2 v_2 \right\} \tag{3.8}$$

Energy balance equation is expressed as Eq. 3.9.

$$\dot{E}_k + \dot{E}_p = \dot{W}_{ext} \tag{3.9}$$

From the Newton's second law, the stress terms are expressed by Eq. 3.10.

$$\sigma_1 - \sigma_2 = \rho_s l_s \left(\dot{v}_2 + 0.5\dot{v}_d \right) \tag{3.10}$$

By substituting Eq. 3.5, 3.7 and 3.8 to Eq. 3.9, and solving Eq. 3.9 and Eq. 3.10 simultaneously, the average axial stress in the specimen can be obtained as Eq. 3.11. Because of the assumption 4, the strength is enhanced by not material effect but structural effects, which are the inertia effects expressed by Eq. 3.12.

$$\begin{aligned} \sigma_{avg} = E_s \varepsilon_x + \ddot{\varepsilon}_x \rho_s \left[\frac{v_s^{\,2} d_s^{\,2}}{8} + \frac{l_s^{\,2}}{12} \right] \\ + \dot{\varepsilon}_x^{\,2} \rho_s \left[\frac{v_s^{\,2} d_s^{\,2}}{16} - \frac{v_s^{\,3} d_s^{\,2}}{4} + \frac{l_s^{\,2}}{4} - \frac{v_s l_s^{\,2}}{3} \right] + v_1 v_2 \rho_s \left(\frac{1}{2} - v_s \right) \end{aligned} \tag{3.11}$$

$$\begin{aligned} \Delta\sigma_{inertia} = \ddot{\varepsilon}_x \rho_s \left[\frac{v_s^{\,2} d_s^{\,2}}{8} + \frac{l_s^{\,2}}{12} \right] \\ + \dot{\varepsilon}_x^{\,2} \rho_s \left[\frac{v_s^{\,2} d_s^{\,2}}{16} - \frac{v_s^{\,3} d_s^{\,2}}{4} + \frac{l_s^{\,2}}{4} - \frac{v_s l_s^{\,2}}{3} \right] + v_1 v_2 \rho_s \left(\frac{1}{2} - v_s \right) \end{aligned} \tag{3.12}$$

As shown in Eq. 3.12, the factors influencing the inertia effects in dynamic material test are strain acceleration, strain rate, geometrical properties of a specimen, and velocities on the interfaces between the specimen and the bar components. In order to find out the key factors among these factors, the inertia effect terms were evaluated for seventy-two cases of

concrete SHPB tests dealt with in chapter 3.2 as shown in Table 3.1. Results in Table 3.1 show the strain rate and the interfaces velocities terms ratio to strain acceleration term, and it was confirmed that strain rate and interfaces velocities terms are much smaller than strain acceleration term. Therefore, the key factors for the inertia effects in concrete SHPB test are strain acceleration, dimension, and density of a specimen.

Table 3.1 Comparison between inertia effects terms in concrete SHPB tests

	$\left[\dot{\varepsilon}_x^{\,2}\left(d_s^{\,2}+l_s^{\,2}\right)\right]/\left[\ddot{\varepsilon}_x\left(d_s^{\,2}+l_s^{\,2}\right)\right]$	$v_1 v_2 / \left[\ddot{\varepsilon}_x\left(d_s^{\,2}+l_s^{\,2}\right)\right]$
Mean	0.95 %	0.16 %
Range	0.22 – 2.65 %	0.03 – 1.21 %

3.1.2. Rate effect and inertia effects in apparent DIF

Dynamic strength enhancement in apparent DIF can be separated by the rate effect and the inertia effects such as Eq. 3.13. Then, Eq. 3.13 can be expressed by DIF due to the pure rate effect and strength enhancement due to the inertia effects such as Eq. 3.14.

$$DIF_{apparent} = \frac{f_{c,static} + \Delta f_c}{f_{c,static}} = \frac{f_{c,static} + \Delta f_{rate} + \Delta f_{inertia}}{f_{c,static}} \tag{3.13}$$

$$DIF_{apparent} = DIF_{rate} + \frac{\Delta f_{inertia}}{f_{c,static}} \tag{3.14}$$

Meanwhile, Mihashi and Wittmann (1980) suggested that the rate effect of concrete can be expressed by a power function like Eq. 3.15. $\dot{\sigma}$, $\dot{\sigma}_0$, and β denote loading rate of concrete, reference loading rate, and material parameter. After that, Eq. 3.15 has been used to describe the rate effect of concrete in the rate theory which explains crack propagation by bond and unbond between atoms or molecules (fib Commission 8 2013).

$$DIF_{rate} = \left(\frac{\dot{\sigma}}{\dot{\sigma}_0} \right)^{\frac{1}{\beta+1}} \tag{3.15}$$

In this study, DIF considering the pure rate effect was expressed by a power function of strain rate as Eq. 3.16 as similar to DIF of fib MC2010 considering that DIF is defined as a function of strain rate in many material models. Also, this is valid because it was reported that Young's modulus is relatively rate independent (ACI Committee 370). $\dot{\varepsilon}_s$, $\dot{\varepsilon}_{s,static}$, and k_1 denote strain rate of specimen, reference strain rate, and a parameter for DIF considering the pure rate effect.

$$DIF_{rate} = \left(\frac{\dot{\varepsilon}_s}{\dot{\varepsilon}_{s,static}} \right)^{k_1} \tag{3.16}$$

Reference strain rate was determined to be 10^{-5} s^{-1} by referring ASTM C39/C39M-16b.

Furthermore, from the result of chapter 3.1.1, the dynamic strength enhancement due to the inertia effects can be assumed as Eq. 3.17 with the

key factors. k_2, and k_3 denote parameters related with the radial and axial inertia effects.

$$\Delta f_{inertia} = k_2 \rho_s {d_s}^2 \ddot{\varepsilon}_s + k_3 \rho_s {l_s}^2 \ddot{\varepsilon}_s \tag{3.17}$$

According to Forrestal et al. (2007), the confining pressure due to the radial inertia effects is also expressed by the term of diameter, density, and strain acceleration of a specimen, which is the same as the first term of the right side in Eq. 3.17. Moreover, the strength enhancement due to the confining effect is linear to the confining pressure (Macgregor and Wight 2011). Therefore, Eq. 3.17 also includes the confining effect due to radial inertia effects.

Therefore, apparent DIF in SHPB test is expressed with three regression parameters such as Eq. 3.18. Eq. 3.18 is reasonable because geometrical properties, which are not material properties, are only included in the inertia effects, which are structural effects.

$$DIF_{apparent} = \left(\frac{\dot{\varepsilon}_s}{\dot{\varepsilon}_{s,static}} \right)^{k_1} + k_2 \frac{\rho_s {d_s}^2}{f_{c,static}} \ddot{\varepsilon}_s + k_3 \frac{\rho_s {l_s}^2}{f_{c,static}} \ddot{\varepsilon}_s \tag{3.18}$$

In conclusion, the key factors causing the inertia effects were determined, and the apparent DIF, which consists of these factors, was mathematically formulated by considering energy balancing conditions. Actually, this model was based on a linear elastic material, which cannot fully represent the properties of concrete. However, in this study, three regression parameters in Eq. 3.18 were determined based on the results of concrete SHPB tests. By doing this, the properties of concrete were indirectly considered in Eq. 3.18.

3.2. Concrete SHPB Test

In order to obtain test data of concrete SHPB test for regression analysis of Eq. 3.18, concrete SHPB tests were conducted. Because the inertia effects in apparent DIF are influenced by static strength, diameter, length of specimen, and strain acceleration, these factors were selected as test variables. However, because density is almost constant for normal weight concrete, it was not included in test variables. Table 3.2 shows the test variables, which are divided into specimen characteristics and SHPB test conditions. Twelve specimen groups were set up with specimen characteristics such as static strength, diameter, and L/D ratio of specimens as shown in Table 3.2, and each group was tested with six strain rate and strain acceleration combinations. The I.D. of specimen groups was defined as Sxx-Dyy-Lzz. xx, yy, and zz denote static strength from standard cylinder specimen compressive test, diameter, and length of a specimen. SHPB test conditions were determined by performing pre-analyses with LS-DYNA to control strain rate region and to satisfy dynamic equilibrium of specimens.

Table 3.2 Variables of concrete SHPB test

Specimen characteristics (12)			SHPB test conditions (6)		
f_c', MPa	Diameter, mm	L/D ratio	Striker length, mm	Impact velocity, m/s	Pulse shaper
52, 61, 85	50, 75	0.5, 1	200, 300, 600	12 – 20	Individual design

3.2.1. Specimen preparation

Table 3.3 indicates concrete mix proportion. Considering small dimension of SHPB test specimens, maximum aggregate size was determined to be 13 mm. Also, high range water reducing admixture was used. In the case of specimens for static strength test, concrete was placed in D150×H300 standard cylinder molds, and in the case of specimens for SHPB test, D50×H100 and D75×H150 cylinder molds were used. Specimens were demolded after 24 hours. After that, specimens were cured in the constant temperature and humidity chamber for 28 days. After curing, specimens for SHPB test were cut and ground. Figure 3.2, 3.3, and 3.4 shows the SHPB test specimens.

Table 3.3 Concrete mix proportion

f_c', MPa	G_{max}, mm	W/B, %	S/a, %	Unit weight, kg/m^3					
				W	C	SF*	S	G	Adx
52	13	34	44	176	520	-	715	918	5.2
61	13	36	40	173	480	-	676	1014	4.8
85	13	25	41	160	590	51.3	604	868	6.41

* Silica Fume

Figure 3.2 52 MPa concrete SHPB test specimens

Figure 3.3 61 MPa concrete SHPB test specimens

Figure 3.4 85 MPa concrete SHPB test specimens

Static strength is needed to define DIF as shown in Eq. 1.2, so static tests were conducted. Loading rate was determined to be 0.003 mm/s to satisfy reference strain rate in Eq. 3.16. Test results are listed in Table 3.4.

Table 3.4 Results of standard cylinder compressive tests

f_c', MPa	Density, kg/m^3	Poisson ratio
51.90	2,400	0.1904
61.35	2,407	0.1840
85.10	2,449	0.1921

3.2.2. SHPB test procedure

76.2 mm SHPB of Extreme Performance Testing Center in Seoul National University in Figure 3.5 was used for SHPB test. This apparatus was made with high strength alloy steel (AISI 4140 alloy steel). The properties of bar components are listed in Table 3.5.

SHPB test conditions are listed in Table 3.6. These are determined by pre-analyses with LS-DYNA. Heard et al. (2014) suggested that high frequency components in an incident stress wave due to the radial inertia effect in a pulse shaper can be reduced by using annular pulse shaper rather than solid disk pulse shaper. For this reason, C10200 copper annular pulse shaper was designed and applied to SHPB test as shown in Figure 3.6. In addition, petroleum jelly was applied to surfaces of pulse shaper and specimen to minimize frictional effect. Figure 3.7 and 3.8 show the specimen of S52-D75-L38 test 4 before and after the test. Strain gauges, whose gauge length was 3 mm by referring Ueda and Umeda (1998), were attached to the surfaces of the incident and transmitted bars to measure incident, reflected, and transmitted waves. Using the gauges, strain was measured with the sampling rate of 1 MHz. Moreover, high speed camera was used to observe fracture pattern of a specimen and check whether a specimen was properly settled between the two bars during the tests. Figure 3.9 shows a fracture pattern of S52-D75-L38 test 3 from high speed camera. In Figure 3.9, specimens were fractured by splitting due to tension in the radial direction, which is desirable for determining DIF (Zhang et al. 2011).

Table 3.5 Geometrical and material properties of bar components

	Properties	Incident & transmitted bars
Geometrical properties	Diameter, mm	76.2
	Length, m	5.5
Material properties	Density, kg/m^3	7850
	Young's modulus, GPa	205
	Yield strength, MPa	485
	Poisson ratio	0.29

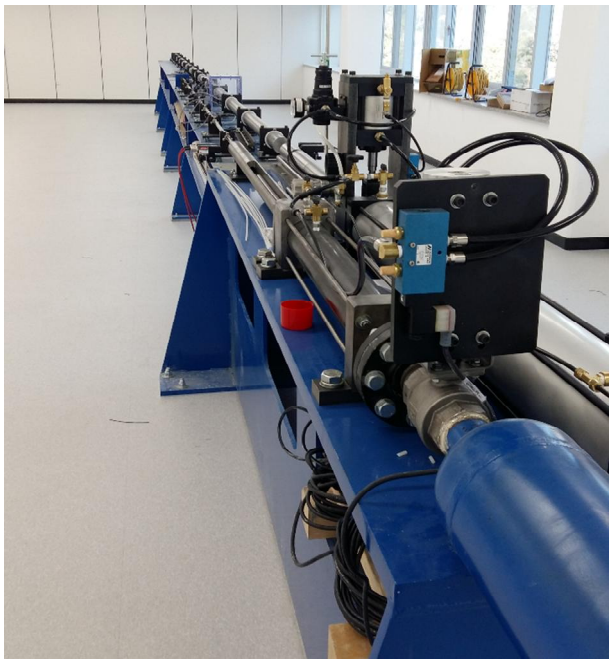

Figure 3.5 SHPB system of EPTC in SNU

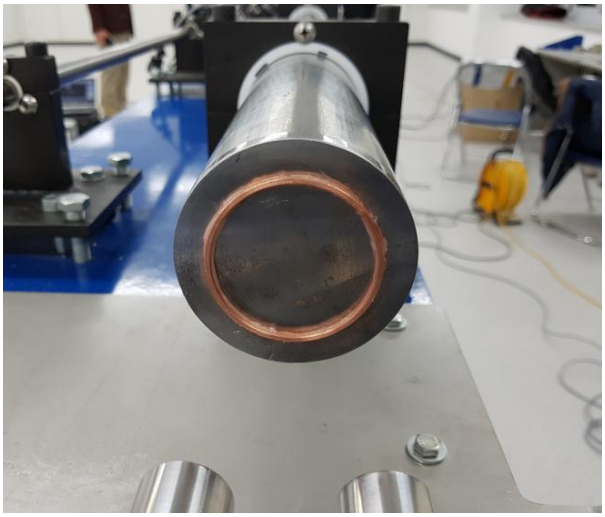

Figure 3.6 Annular pulse shaper

Figure 3.7 Specimen of S52-D75-L38 test 4 before SHPB test

Figure 3.8 Specimen of S52-D75-L38 test 4 after SHPB test

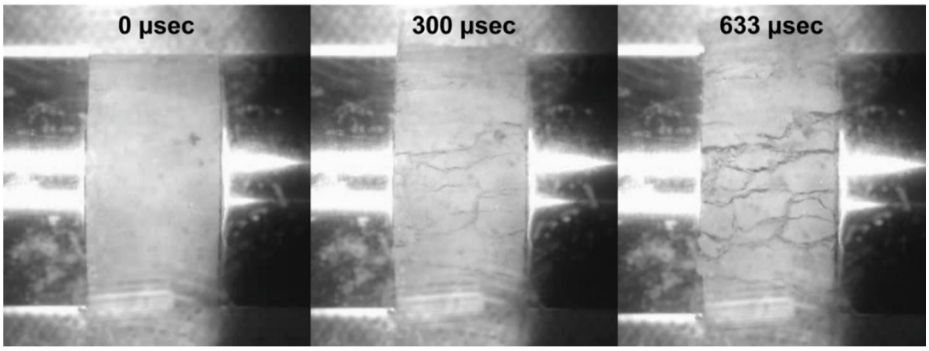

Figure 3.9 Fracture pattern of S52-D75-L38 test 3

Table 3.6 Concrete SHPB test conditions

#	I.D.	Striker length, mm	Impact velocity, m/s	Pulse shaper, mm (O. Dia.×I. Dia.×T.)
1	S52-D50-L25	200	12	55×51×3
2			16	
3			20	
4			18	55×51×2
5			18	55×48×2
6			20	
1	S52-D50-L50	200	12	55×51×3
2			16	
3			20	
4			18	55×51×2
5			18	55×48×2
6			20	
1	S61-D50-L25	200	12	55×51×3
2			16	
3			20	
4			18	55×51×2
5			18	55×48×2
6			20	
1	S61-D50-L50	200	12	55×51×3
2			16	
3			20	
4		300	18	55×51×2
5		200	18	55×48×2
6			20	
1	S85-D50-L25	200	12	55×51×3
2			16	
3			20	
4			18	55×51×2
5			18	55×48×2
6			20	
1	S85-D50-L50	300	12	55×51×3
2		200	16	
3			20	
4			18	55×51×2
5			18	55×48×2
6			20	

#	I.D.	Striker length, mm	Impact velocity, m/s	Pulse shaper, mm (O. Dia.×I. Dia.×T.)
1	S52-D75-L38	600	12	55×51×3
2		300	16	
3			16	55×48×3
4			18	
5			18	55×48×2
6			20	55×45×2
1	S52-D75-L75	600	12	55×51×3
2		300	16	
3			16	55×45×3
4			18	
5			18	
6			20	
1	S61-D75-L38	600	12	55×51×3
2		300	16	
3			16	55×48×3
4			18	
5			18	55×48×2
6			20	55×45×2
1	S61-D75-L75	600	12	55×51×3
2		300	16	
3			16	55×45×3
4			18	
5			18	55×45×2
6			20	
1	S85-D75-L38	600	12	55×51×3
2		300	16	
3			18	55×48×2
4			18	55×45×3
5			20	
6			20	55×45×2
1	S85-D75-L75	600	12	55×51×3
2		300	16	
3			16	55×45×3
4			18	
5			18	55×45×2
6			20	

3.2.3 Concrete SHPB test results

Stress waves on incident and transmitted bars were measured as shown in Figure 3.10. Then, the data was filtered by low pass filter as shown in Figure 3.11. The cut-off frequency was determined to be 20 kHz because response components at the frequencies over 20 kHz are negligible as shown in Figure 3.12.

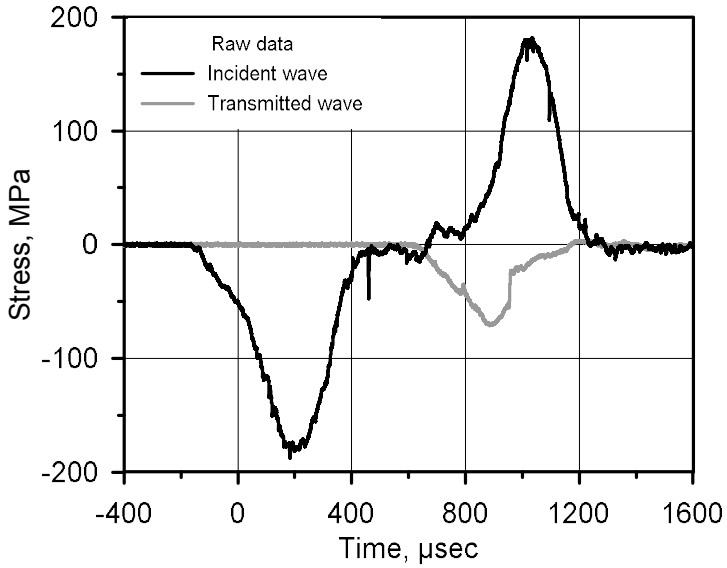

Figure 3.10 Raw data of S52-D75-L38 test 1

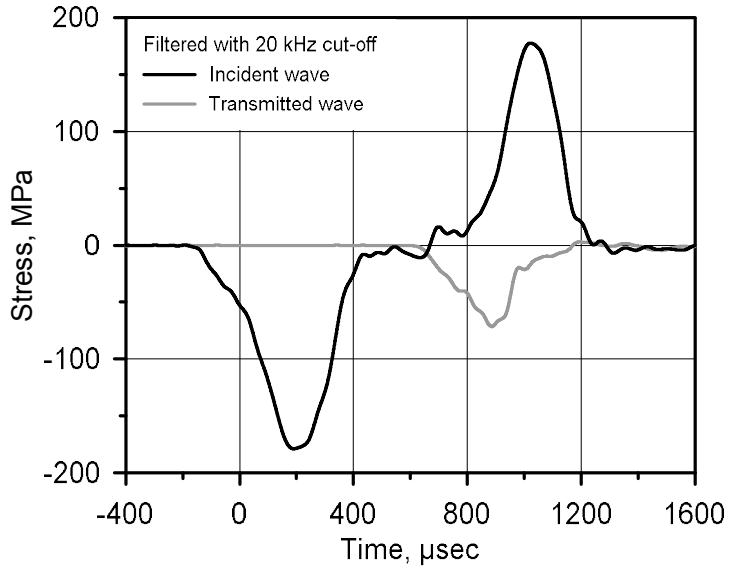

Figure 3.11 Filtered data of S52-D75-L38 test 1 with 20 kHz low pass filter

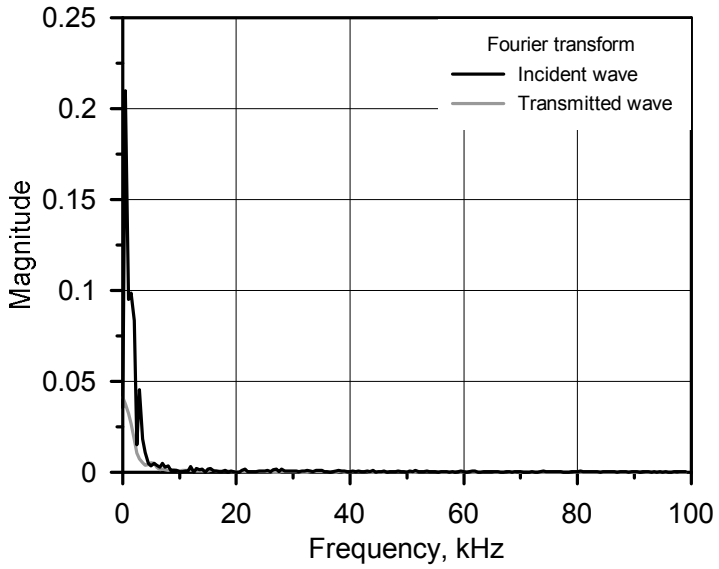

Figure 3.12 Fourier transform of raw data of S52-D75-L38 test 1

After that, the stress waves were shifted as shown in Figure 3.13, and strain rate, strain, and stress were obtained by using Eq. 2.7, 2.8, and 2.11 as shown in Figure 3.14. In addition, strain acceleration was calculated by central difference method as Eq. 3.19.

$$\ddot{\varepsilon}_{s,i} = \frac{\dot{\varepsilon}_{s,i+1} - \dot{\varepsilon}_{s,i-1}}{t_{i+1} - t_{i-1}} \tag{3.19}$$

Finally, Figure 3.15 and 3.16, and Table 3.7 indicate all concrete SHPB test results in this study. Apparent DIF was calculated by dividing the apparent dynamic strength by static strength from standard cylinder specimen compressive test.

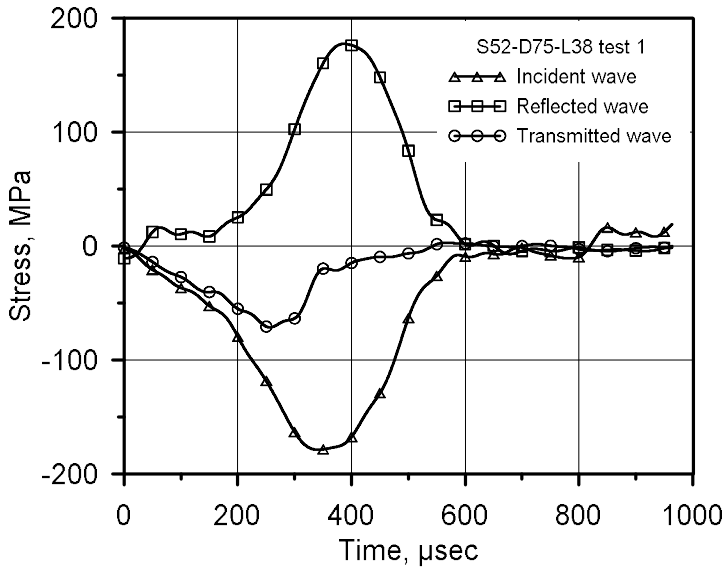

Figure 3.13 Stress waves of S52-D75-L38 test 1

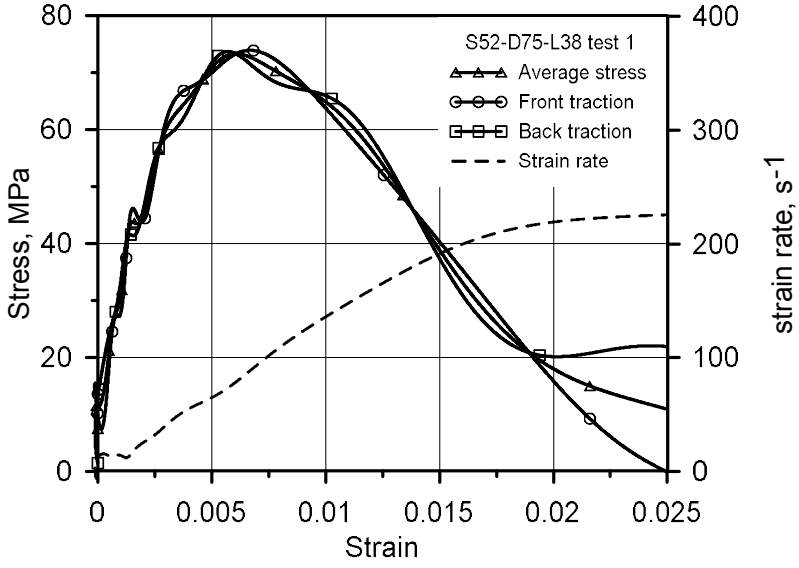

Figure 3.14 Dynamic stress-strain curve of S52-D75-L38 test 1

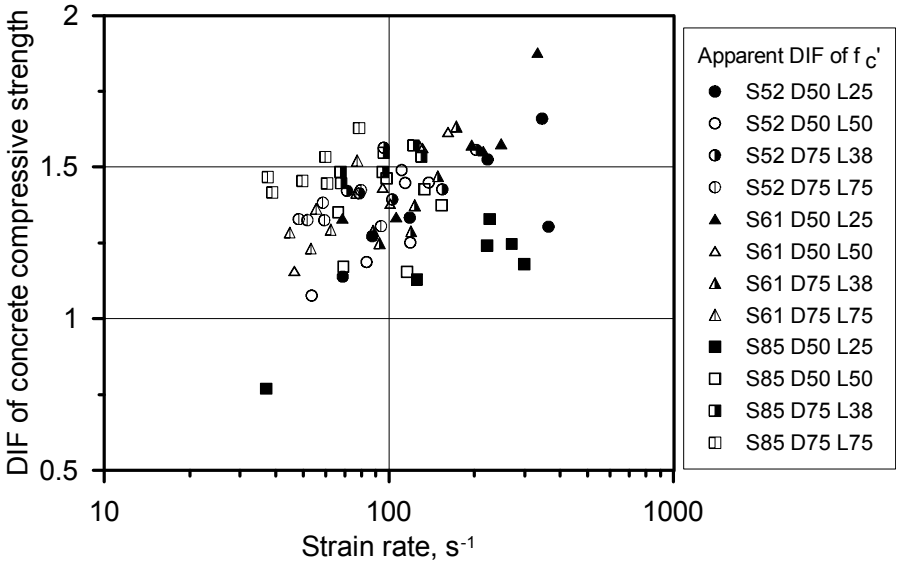

Figure 3.15 Apparent DIF from SHPB test results

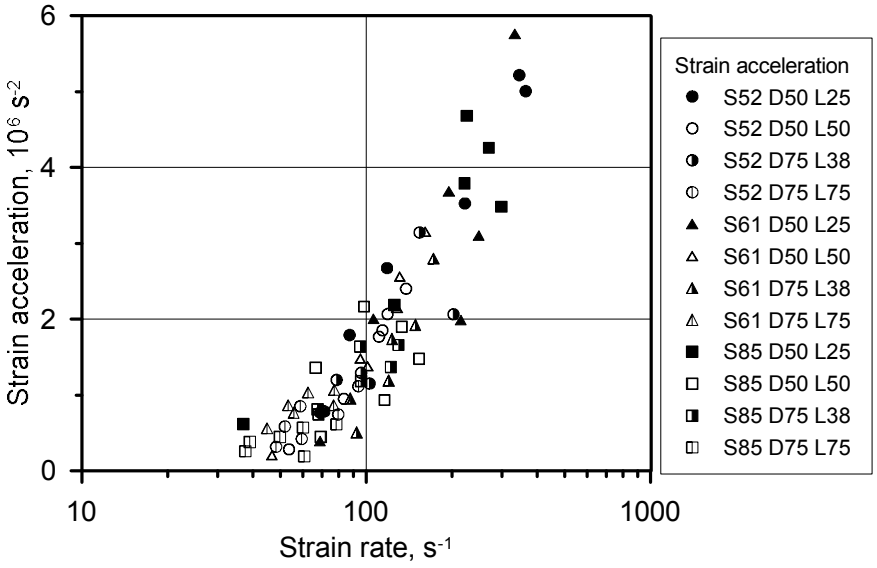

Figure 3.16 Strain acceleration from SHPB test results

Table 3.7 Concrete SHPB test results

#	I.D.	Apparent DIF	Strain rate, s^{-1}	Strain acceleration, s^{-2}
1	S52-D50-L25	1.1388	68.82	769,651
2		1.2723	87.34	1,790,607
3		1.3335	118.36	2,673,615
4		1.3035	364.01	5,006,696
5		1.5250	222.41	3,526,572
6		1.6599	345.44	5,217,991
1	S52-D50-L50	1.0766	53.52	283,086
2		1.1871	83.44	948,884
3		1.4903	110.80	1,768,478
4		1.2513	118.87	2,067,414
5		1.4479	114.03	1,852,835
6		1.4491	138.03	2,401,414
1	S61-D50-L25	1.3312	68.68	390,062
2		1.3352	106.08	2,005,805
3		1.5728	195.31	3,683,602
4		1.8773	332.67	5,762,906
5		1.5521	215.00	1,988,291
6		1.5769	248.56	3,105,222
1	S61-D50-L50	1.1581	46.51	209,806
2		1.4331	95.19	1,481,217
3		1.5639	131.21	2,559,665
4		1.6166	161.46	3,153,717
5		1.3787	101.00	1,382,908
6		1.5694	128.20	2,146,352
1	S85-D50-L25	0.7697	36.99	615,463
2		1.1301	125.52	2,188,795
3		1.2465	270.09	4,260,208
4		1.3290	226.00	4,681,271
5		1.2419	221.69	3,793,394
6		1.1804	298.74	3,484,640
1	S85-D50-L50	1.1721	69.06	448,297
2		1.3512	66.31	1,360,111
3		1.4630	98.08	2,164,603
4		1.4273	133.38	1,900,448
5		1.1553	115.88	934,606
6		1.3747	153.20	1,478,677

#	I.D.	Apparent DIF	Strain rate, s^{-1}	Strain acceleration, s^{-2}
1	S52-D75-L38	1.4133	78.67	1,198,861
2		1.5640	95.83	1,292,231
3		1.4218	71.23	784,089
4		1.3935	102.70	1,151,152
5		1.4267	154.04	3,143,498
6		1.5568	202.82	2,064,067
1	S52-D75-L75	1.3254	51.69	584,347
2		1.3827	58.57	851,339
3		1.3286	48.18	316,820
4		1.3251	59.27	420,064
5		1.4243	79.65	742,399
6		1.3054	93.77	1,115,445
1	S61-D75-L38	1.2904	87.91	953,579
2		1.3741	123.34	1,740,925
3		1.2493	92.55	507,017
4		1.2886	119.78	1,191,774
5		1.6335	172.59	2,798,375
6		1.4706	148.81	1,923,402
1	S61-D75-L75	1.3628	55.56	768,177
2		1.5215	77.19	1,067,583
3		1.2850	44.76	562,325
4		1.2321	53.14	865,723
5		1.2941	62.38	1,034,256
6		1.4153	76.70	867,004
1	S85-D75-L38	1.4475	67.91	745,117
2		1.4837	95.20	1,639,295
3		1.5714	122.04	1,367,875
4		1.4846	67.51	810,555
5		1.5470	95.78	1,184,472
6		1.5353	130.00	1,660,570
1	S85-D75-L75	1.4164	38.88	381,190
2		1.5334	59.80	568,830
3		1.4671	37.49	258,211
4		1.4544	49.61	448,738
5		1.4459	60.52	188,681
6		1.6291	78.52	613,692

3.3 Suggestion for DIF Considering the Pure Rate Effect

Regression analysis of Eq. 3.18, which indicates apparent DIF, was performed with the test results in chapter 3.2.3 by using Least Square Error Method. The objective function was set up as the sum of square error such as Eq. 3.20.

$$\Pi = \frac{1}{2}\sum_i \left[DIF_{test,i} - \left\{ \left(\frac{\dot{\varepsilon}_s}{\dot{\varepsilon}_{s,static}} \right)^{k_1} + k_2 \frac{\rho_s {d_s}^2 \ddot{\varepsilon}_s}{f_{c,static}} + k_3 \frac{\rho_s {l_s}^2 \ddot{\varepsilon}_s}{f_{c,static}} \right\}_i \right]^2 \quad (3.20)$$

At a critical point of Eq. 3.20, Eq. 3.21 should be valid.

$$\nabla_{\mathbf{k}} \Pi = \mathbf{0} \quad (3.21)$$

Meanwhile, the first component of the gradient of Π is nonlinear function as shown in Eq. 3.22. Therefore, Newton-Rapson method was applied to obtain a minimum point as shown in Eq. 3.23.

$$\begin{aligned} f &= \frac{\partial \Pi}{\partial k_1} = \sum_i \left[\left\{ A_i^{k_1} + k_2 B_i + k_3 C_i - DIF_{test,i} \right\} A_i^{k_1} \ln A_i \right] = 0 \\ \text{where, } A_i &= \frac{\dot{\varepsilon}_{s,i}}{\dot{\varepsilon}_{s,static}},\ B_i = \frac{{d_{s,i}}^2 \rho_{s,i}}{f_{c,static,i}} \ddot{\varepsilon}_{s,i},\ C_i = \frac{{l_{s,i}}^2 \rho_{s,i}}{f_{c,,static,i}} \ddot{\varepsilon}_{s,i} \end{aligned} \quad (3.22)$$

$$k_{1,i+1} = k_{1,i} - f\left(k_{1,i}\right) \left(\left. \frac{df}{dk_1} \right|_{k_1 = k_i} \right)^{-1} \quad (3.23)$$

It was confirmed that there is the unique solution as shown in Figure 3.17. Furthermore, Hessian of Π was checked to confirm that the critical point calculated is the minimum such as Eq. 3.24.

$$\left.\frac{\partial^2 \Pi}{\partial k_1^{\,2}}\right|_{\mathbf{k}} > 0 \;\;\&\;\; \det \mathbf{H}\big|_{\mathbf{k}} > 0 \tag{3.24}$$

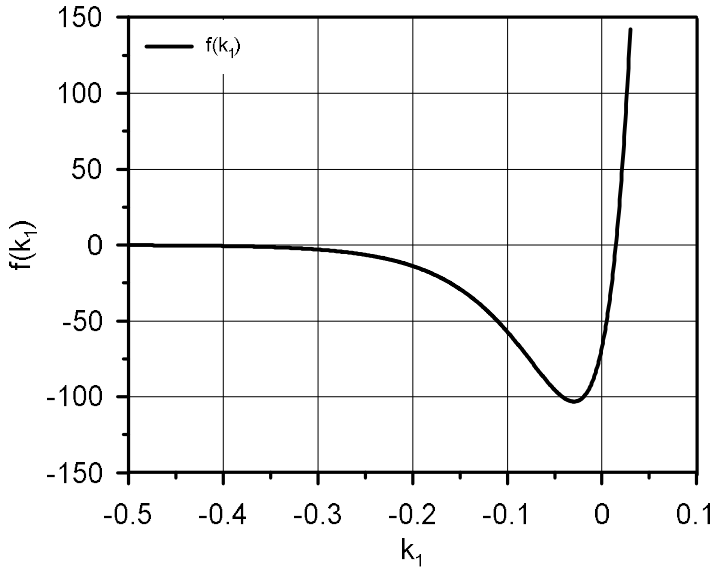

Figure 3.17 The first components of the gradient of Π along k_1

Finally, apparent DIF was obtained as Eq. 3.25. In order to make **k** dimensionless, the units of variables were set up as Table 3.8.

$$DIF_{apparent} = \left(\frac{\dot{\varepsilon}_s}{10^{-5}}\right)^{0.0147} + 0.3501\frac{d_s^{\,2}\rho_s\ddot{\varepsilon}_s}{f_{c,static}} + 0.4100\frac{l_s^{\,2}\rho_s\ddot{\varepsilon}_s}{f_{c,static}} \tag{3.25}$$

Table 3.8 Units of variables

Variables	$\dot{\varepsilon}_s$	$\ddot{\varepsilon}_s$	ρ_s	$f_{c,static}$	d_s	l_s
Units	s^{-1}	s^{-2}	kg/m^3	Pa	m	m

DIF due to the pure rate effect can be obtained by subtracting the inertia effects from apparent DIF. Therefore, DIF due to the pure rate effect is expressed as Eq. 3.26. Figure 3.18 indicates the proposed and representative DIFs.

$$DIF_{rate} = \left(\frac{\dot{\varepsilon}_s}{10^{-5}} \right)^{0.0147} \tag{3.26}$$

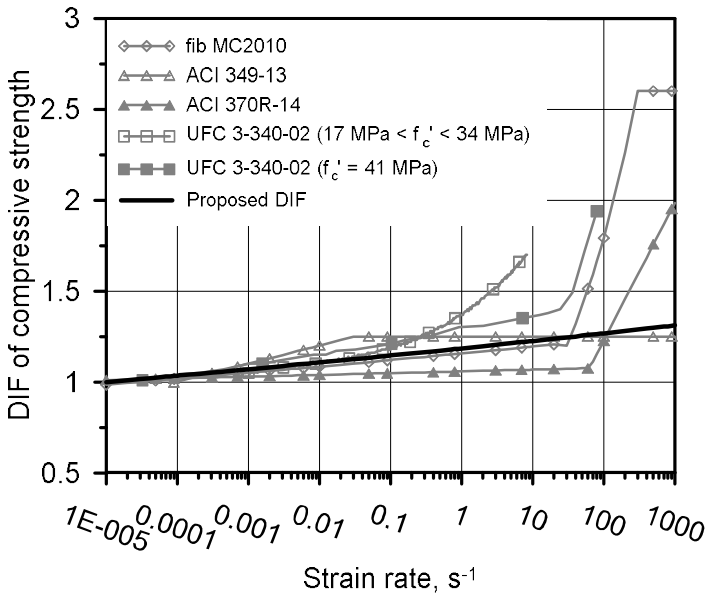

Figure 3.18 Proposed and representative DIFs

4. Verification of Proposed DIF

In this chapter, proposed DIF was verified by performing FEA for concrete SHPB tests in chapter 3.2 with LS-DYNA. Also, the other representative DIFs were applied to analyses for comparison with analyses results of proposed DIF. As a result, apparent dynamic strength ratio was obtained, and the results were discussed.

4.1 Verification Analyses Modeling

In order to verify proposed DIF, FEA with proposed and representative DIFs were conducted for all concrete SHPB tests in chapter 3.2 by LS-DYNA. In the case of DIF of UFC 3-340-02, DIF for 41 MPa was applied. As shown in Figure 4.1, only specimen, incident and transmitted bars were modeled, and the load curves from the test results were applied as described nodal forces to the incident bar instead of striker bar and pulse shaper modeling. As same as post-processing of SHPB test, the strain waves of the incident and transmitted bars along time were obtained and post-processed by using Eq. 2.7, 2.8, 2.11, and 3.19.

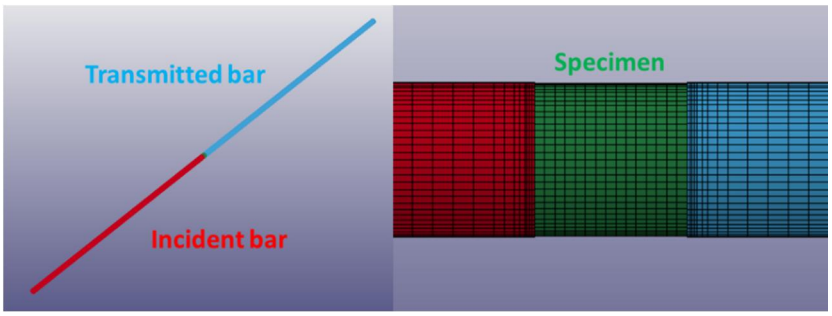

Figure 4.1 FE model of S52-D75-L75 test 2

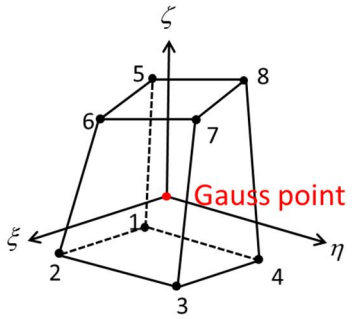

Figure 4.2 Eight nodes solid hexahedron element with one integration point

Eight nodes solid hexahedron element was adopted as element type, and integration was carried out by one point Gaussian quadrature rule as shown in Figure 4.2. The material model of bar components was adopted as linear elastic model because the bar components remained elastic, and the material model of concrete specimen was 72R3 concrete damage model suggested by Malvar et al. (1997) and Magallanes et al. (2010). This model is targeted at reinforced concrete structures subjected to blast and impact loading, and it has the advantage that it is easy to apply various DIFs to the constitutive equation.

As results of analyses, dynamic stress-strain curves were obtained as shown in Figure 4.3. Finally, apparent strength ratio was evaluated such as Eq. 4.1 for verification of proposed DIF. Apparent strength ratio close to 1.0 implies that the result of FEA gives a good prediction for the test result, and the ratio larger than 1.0 means that the result of FEA overestimates the test result.

$$\text{Apparent strength ratio} = \frac{\left(\text{Apprent dynamic strength from FEA}\right)}{\left(\text{Apprent dynamic strength from SHPB test}\right)} \quad (4.1)$$

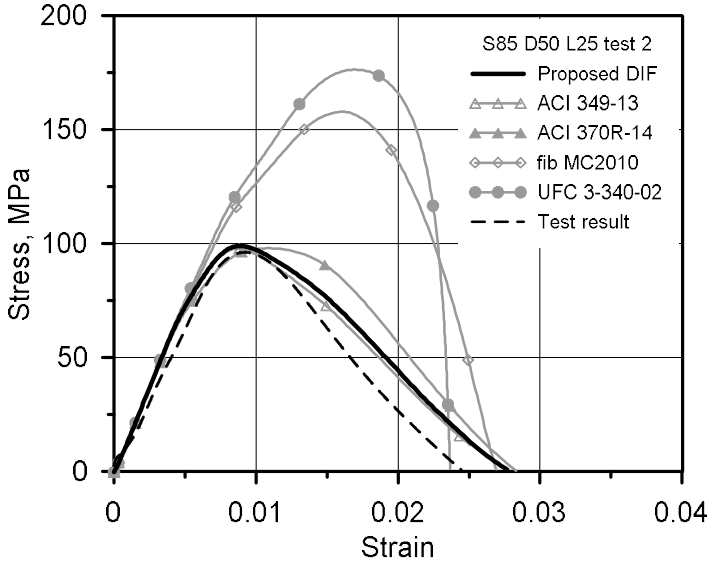

Figure 4.3 Stress-strain curves of S85-D50-L25 test 2 from analyses and test

4.2 Verification Results and Discussion

4.2.1 Verification results

Figure 4.4, 4.5, and 4.6 show calculated apparent strength ratio for all analysis result, its mean value for each specimen group, and its mean value for each DIF respectively. Mean and C.O.V. of apparent strength ratio for each DIF are listed in Table 4.1. As known from Table 4.1, proposed DIF predicted apparent dynamic strength of SHPB test with high accuracy. In addition, DIFs of ACI 349-13 and ACI 370R-14 gave similar results to that of proposed DIF also, but C.O.V. of ACI 370R-14 was larger than those of proposed DIF and DIF of ACI 349-13. DIFs of fib MC2010 and UFC 3-340-02 overestimated apparent dynamic strength, and apparent strength ratios were dispersed widely.

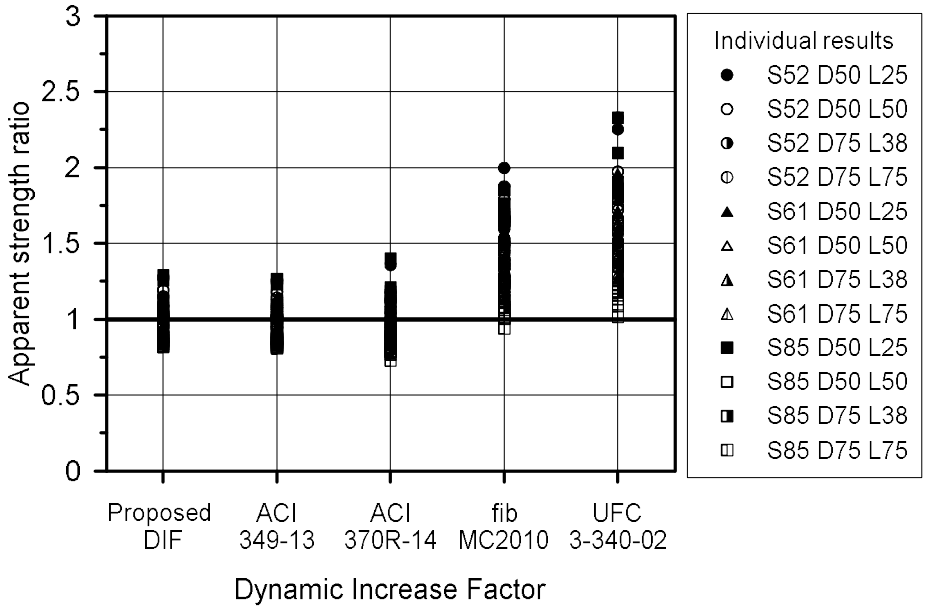

Figure 4.4 Apparent strength ratio for individual analysis result

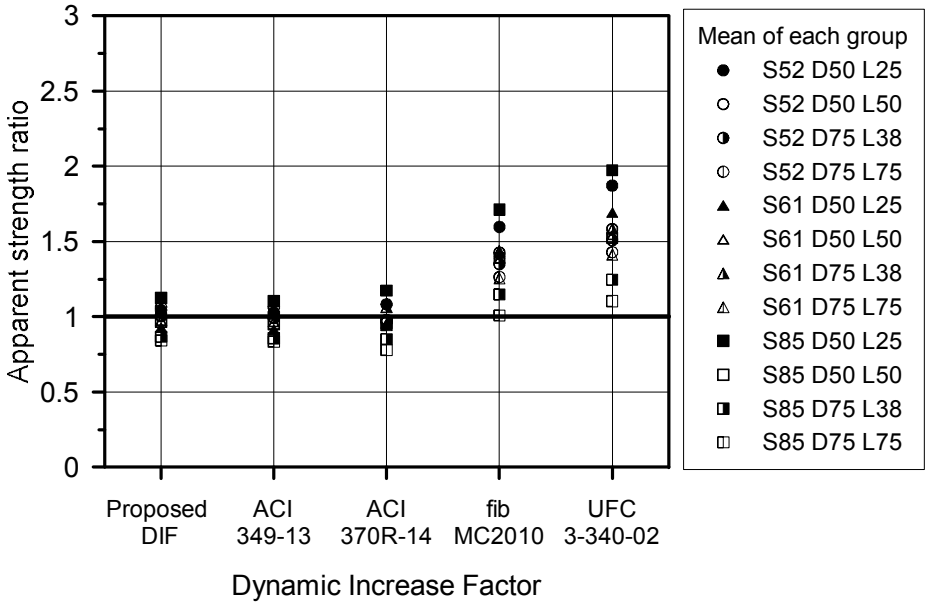

Figure 4.5 Mean apparent strength ratio for each specimen group

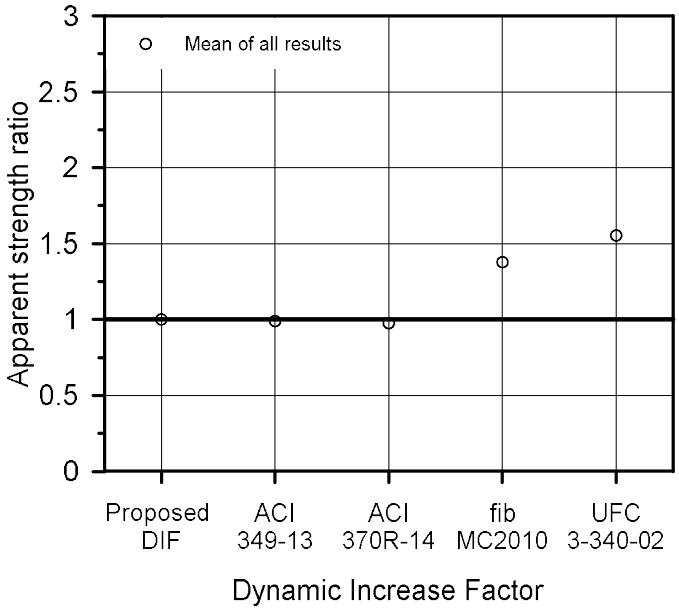

Figure 4.6 Mean apparent strength ratio for all analyses results

Table 4.1 Mean and C.O.V. of apparent strength ratio in accordance with DIFs

	Proposed DIF	ACI 349-13	ACI 370R-14	fib MC2010	UFC 3-340-02
Mean	1.00	0.99	0.98	1.38	1.55
C.O.V.	0.11	0.11	0.14	0.16	0.18

4.2.2 Discussion on verification

4.2.2.1 ACI 349-13

DIF of ACI 349-13 predicted apparent dynamic strength well, but it does not mean that DIF of ACI 349-13 represents DIF considering the pure rate effect. Actually, the similarity between the results of proposed DIF and DIF of ACI 349-13 was caused by the similarity between DIF values of both at tested strain region in this study as shown in Figure 4.7. However, DIF value of ACI 349-13 at the strain rate region is a just meaningless upper limit. The main part of the test data for DIF of ACI 349-13 is ranged under 0.01 s^{-1} strain rate as shown in Figure 4.7, and the test data at higher strain rate was insufficient. Therefore, ACI 349-13 limits DIF value to 1.25.

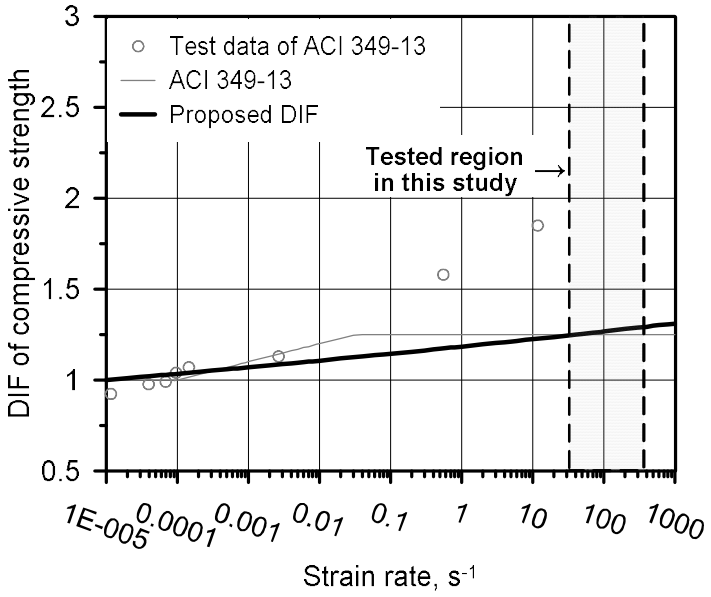

Figure 4.7 Test data for DIF of ACI 349-13 (Newmark and Haltiwanger 1962)

4.2.2.2 ACI 370R-14

In the case of ACI 370R-14, DIF value is smaller than proposed DIF value in the strain rate region under about 114 s^{-1}, and is larger than proposed DIF value in the region over about 114 s^{-1}. Therefore, DIF of ACI 370R-14 predicted apparent dynamic strength well averagely, but C.O.V. was larger than that of proposed DIF. However, as shown in Figure 4.8, there is no test data at the strain rate region under the transition strain rate in ACI 370R-14. DIF at the region was suggested by just connecting between the point of strain rate at quasi-static state and the point of the lowest strain rate among test results. Therefore, there is no experimental verification for DIF in the region. Furthermore, DIF at the region over the transition strain rate was suggested from the test data including the inertia effects. Therefore, DIF at the region is increased steeply due to the inertia effects, so overestimation becomes dominant as strain rate is increased. For these reasons, DIF of ACI 370R-14 is not also DIF considering the pure rate effect.

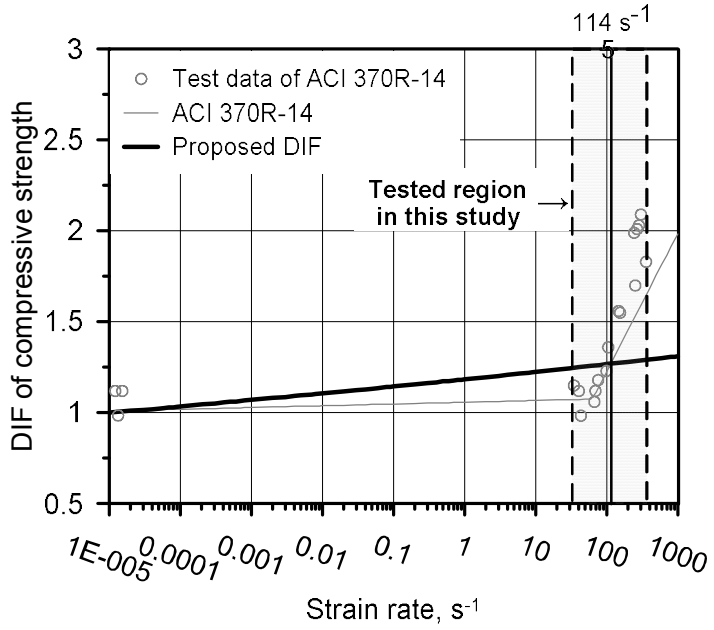

Figure 4.8 Test data for DIF of ACI 370R-14 (Tedesco et al. 1997)

4.2.2.3 fib MC2010 and UFC 3-340-02

As shown in Figure 3.18, DIF of fib MC2010 under the transition strain rate shows the similar tendency to proposed DIF. When it is considered that the steep increase of DIF beyond the transition strain rate is due to the inertia effects, this tendency is corresponded for proposed DIF to exclude the inertia effects from apparent DIF well. However, DIF of fib MC2010 beyond transition strain rate and UFC 3-340-02 overestimated apparent dynamic strength excessively because the DIFs at steep increase region include the inertia effects as known from the verification results.

5. Conclusions

In this study, it was confirmed that the inertia effects in dynamic material test of concrete are influenced by axial strain acceleration, density, and geometrical properties of a specimen. Furthermore, DIF due to the pure rate effect was suggested by performing concrete SHPB tests and nonlinear regression analysis for apparent DIF with the key factors inducing the inertia effects, and proposed DIF was verified by FEA using LS-DYNA for concrete SHPB tests.

DIF of ACI 349-13 predicted apparent dynamic strength of concrete SHPB tests with high accuracy, but because DIF value at the analyzed region was a just meaningless upper limit due to insufficient test data, it is difficult to say that DIF of ACI 349-13 represents DIF considering the pure rate effect. In the case of ACI 370R-14, the prediction was good as focused on mean value, but it does not represent DIF considering the pure rate effect likewise because DIF of ACI 370R-14 includes the inertia effects at the region beyond transition strain rate, and was suggested at the region under transition strain rate without experimental verification by just connecting between the point at quasi-static state and the point at the lowest strain rate tested with the assumption that DIF is a linear function of common logarithm of strain rate. Furthermore, DIFs of fib MC2010 and UFC 3-340-02 overestimated apparent dynamic strength in concrete SHPB tests excessively due to the inertia effects. On the contrary, proposed DIF predicted apparent dynamic strength with high accuracy, and represents DIF considering the pure rate effect well.

Currently, various high performance materials have been developed for construction and reinforcement of structures against extreme events, but those impact and explosion resistance performances have been evaluated without proper considerations about the inertia effects. The methodology correcting the inertia effects from apparent DIF in this study can be extended for evaluation of extreme performance of other cementitious materials. In addition, proposed DIF can be applied to design concrete structures safely and to evaluate safety of concrete structures under extreme events. Therefore, it is expected that results of this study promote researches for safety evaluation and design method development of structures under extreme events.

Reference

ACI Committee 349, “Code Requirements for Nuclear Safety-Related Concrete Structures (ACI 349-13) & Commentary”, Farmington Hills, MI, American Concrete Institute, 2014, pp. 178.

ACI Committee 370, “Report for the Design of Concrete Structures for Blast Effects”, Farmington Hills, MI, American Concrete Institute, 2014, pp. 34.

ASTM C39/C39M-16b, “Standard Test Method for Compressive Strength of Cylindrical Concrete Specimens”, West Conshohocken, PA, ASTM International, 2016, pp. 5.

Bischoff, P. H. and Perry, S. H., “Compressive Behavior of Concrete at High-Strain Rates”, Materials and Structures, Vol. 24, No.144, 1991, pp. 425-450.

Davies, E. and Hunter, S., “The Dynamic Compression Testing of Solids by the Method of the Split Hopkinson Pressure Bar”, Journal of the Mechanics and Physics of Solids, Vol. 11, No.3, 1963 pp. 155-179.

fib Commission 8, “Code-type Models for Concrete Behaviour: State-of-the-art Report”, Vol. 70, Lausanne, fib Fédération internationale du béton, 2013, pp.125.

Forrestal, M., Wright, T., and Chen, W., “The Effect of Radial Inertia on Brittle Samples during the Split Hopkinson Pressure Bar Test”,

International Journal of Impact Engineering, Vol. 34, No.3, 2007, pp. 405-411.

Frew, D., Forrestal, M. J., and Chen, W., "A Split Hopkinson Pressure Bar Technique to Determine Compressive Stress-strain Data for Rock Materials", Experimental Mechanics, Vol. 41, No. 1, 2001, pp. 40-46.

Gorham, D., "Specimen Inertia in High Strain-rate Compression", Journal of Physics D: Applied Physics, Vol. 22, No. 12, 1989, pp. 1888-1893.

Gray, G., Kuhn, H., and Medlin, D., "ASM Handbook, vol. 8, Mechanical Testing and Evaluation", ASM International, Materials Park, 2000, pp. 462-476.

Grote, D., Park, S., and Zhou, M., "Dynamic Behavior of Concrete at High Strain Rates and Pressures: I. Experimental Characterization", International Journal of Impact Engineering, Vol. 25, No. 9, 2001, pp. 869-886.

Hao, Y., Hao, H., Jiang, G. P., and Zhou, Y., "Experimental Confirmation of Some Factors Influencing Dynamic Concrete Compressive Strengths in High-speed Impact Tests", Cement and Concrete Research, Vol. 52, 2013, pp. 63-70.

Heard, W. F., Martin, B. E., Nie, X., and Slawson, T., "Annular Pulse Shaping Technique for Large-Diameter Kolsky Bar Experiments on Concrete", Experimental Mechanics, Vol. 54, No. 8, 2014, pp. 1343-1354.

Kim, D. J., Sirijaroonchai, K., Ek-Tawil, S., and Naaman, A. E., "Numerical Simulation of the Split Hopkinson Pressure Bar Test Technique for Concrete under Compression", International Journal of Impact Engineering, Vol. 37, No. 2, 2010, pp. 141-149.

Li, Q. M., and Meng, H., "About the Dynamic Strength Enhancement of Concrete-like Materials in a Split Hopkinson Pressure Bar Test", International Journal of Solids and Structures, Vol. 40, No. 2, 2003, pp. 343-360.

Li, Q. M., Lu, Y. B., and Meng, H., "Further Investigation on the Dynamic Compressive Strength Enhancement of Concrete-like Materials Based on Split Hopkinson Pressure Bar Tests. Part II: Numerical simulations", International Journal of Impact Engineering, Vol. 36, No. 12, 2009, pp. 1335-1345.

Lok, T. S., Li, X. B., Liu, D., and Zhao, P. J., "Testing and Response of Large Diameter Brittle Materials subjected to High Strain Rate", Journal of Materials in Civil Engineering, Vol. 14, No. 3, 2002, pp. 262-269.

Macgregor, J. G., and Wight, J. K., "Reinforced Concrete: Mechanics and Design", Upper Saddle River, NJ, Pearson Prentice Hall, 2011, pp. 65.

Magallanes, J. M., Wu, Y., Malvar, L. J., and Crawford, J. E., "Recent Improvements to Release III of the K&C Concrete Model", Proceedings of 11th international LS-DYNA Users conference, Livermore Software Technology Corporation, Livermore, CA, 2010.

Malvar, L. J., Crawford, J. E., Wesevich, J. W., and Simons D., "A Plasticity Concrete Material Model for DYNA3D", International Journal of Impact Engineering, Vol. 19, No. 9-10, 1997, pp. 847-873.

Mihashi, H., and Wittmann, F. H., "Stochastic Approach to Study the Influence of Rate of Loading on Strength of Concrete", Heron, Vol. 25, No. 3, 1980, pp. 26-28.

Newmark, N. M., and Haltiwanger, J. D., "Air Force Design Manual, Principles and Practices for Design of Hardened Structures", DTIC Document, 1962.

Samanta, S. K., "Dynamic Deformation of Aluminium and Copper at Elevated Temperatures", Journal of the Mechanics and Physics of Solids, Vol. 19, No. 3, 1971, pp. 117-135.

Ross, C. A., Jerome, D. M., Tedesco, J. W., and Hughes, M. L., "Moisture and Strain Rate Effects on Concrete Strength", ACI Materials Journal, Vol. 93, No.3, 1996, pp. 293-300.

Ross, C. A., Thompson, P. Y., and Tedesco, J. W., "Split-Hopkinson Pressure-Bar Tests on Concrete and Mortar in Tension and Compression", ACI Materials Journal, Vol. 86 No. 5, 1989, pp. 475-481.

Tedesco, J. W., Powell, J. C., Ross, C. A., and Hughes, M. L., "A Strain-rate-dependent Concrete Material Model for ADINA", Computers & Structures, Vol. 64, No. 5-6, 1997, pp. 1053-1067.

Ueda, K., and Umeda, A., “Dynamic Response of Strain Gages up to 300 kHz”, Experimental mechanics, Vol. 38, No. 2, 1998, pp. 93-98.

Unified Facilities Criteria (UFC) 3-340-02, “Structures to Resist the Effects of Accidental Explosions”, Washington D.C., U.S. Department of Defense, 2008, pp. 1064-1066.

Wang, L., “Foundations of Stress Waves”, Oxford, Elsevier, 2007, pp. 46.

Zhang, M., Wu, H. J., Li, Q. M., and Huang, F. L., “Further Investigation on the Dynamic Compressive Strength Enhancement of Concrete-like Materials Based on Split Hopkinson Pressure Bar Tests. Part I: Experiments”, International Journal of Impact Engineering, Vol. 36, No. 12, 2009, pp. 1327-1334.

Zhang, M. H., Quek, S. T., and Wang, S., “Effect of Specimen Size on Static Strength and Dynamic Increase Factor of High-Strength Concrete from SHPB Test”, Journal of Testing and Evaluation, Vol. 39, No. 5, 2011, pp. 1-10.

국문초록

순수 변형속도 효과를 고려한
콘크리트 압축강도 동적증가계수

이 상 호

차량, 선박, 항공기 충돌, 폭발, 지진, 쓰나미 등 극단상황 하의 구조물은 일반적으로 정적상태에 비해 높은 변형속도로 하중을 받게 된다. 따라서 극단상황 하 콘크리트 구조물의 경제적인 설계와 정확한 거동 평가를 위해서는 콘크리트의 동적 재료특성을 고려해야만 한다.

한편, 콘크리트는 변형속도 의존특성을 가진 재료로서, 변형률 속도에 따라 압축강도, 인장강도, 임계변형률 등 재료특성이 민감하게 변화한다. 특히, 콘크리트의 동적강도는 변형률 속도가 증가함에 따라 증진되는데, 이는 하중재하시간이 짧아지기 때문에 균열 진전이 어려워진다는 점과 공극 속 자유수가 관성효과를 유발하며 변형에 저항한다는 점 때문이다. 이를 콘크리트 압축강도에 대한 변형속도 효과라 하며, 현재 이를 고려하기 위해서 동적증가계수가 널리 사용되고 있다.

지금까지 많은 동적증가계수가 제안되어 왔으나, 제안된 동적증가계수들은 공통적인 문제점을 가지고 있다. 첫 번째로 동적증가계수를 오직 변형률 속도에 의한 함수로 가정했다. 따라서 정적강도, 변형률 가속도, 시편의 형상 및 크기, 밀도 등 동적 재료물성 실험 시 실험결과에 영향을 줄 수 있는 다른 변수들을 고려하지 않았다. 이에 따라 현재 동적증가계수 실험 데이터는 같은 변형률 속도에서 널리 분산되어 있다. 또한 동적증가계수 실험 데이터에는 축방향 및 반경방향 관성효과에 의한 강도증진이 포함되어 있으나 이를 변형속도 효과에 의한 것으로 간주하였다. 그러나 관성효과는 운동방정식에서 이미 고려하고 있는 효과이기 때문에 이를 동적증가계수를 통해 구성방정식에 반영한다면 중복하여 관성효과를 고려하게 되며 비보수적인 결과를 얻을 수 있다.

본 연구에서는 선형탄성체 시편에 대한 split Hopkinson pressure bar (SHPB) 실험의 해석적 모델로부터 관성효과에 영향을 주는 주요 변수를 선정하였다. 이후 주요 변수를 이용하여 구성한 겉보기 동적증가계수를 콘크리트 SHPB 실험결과를 바탕으로 비선형 회귀분석을 수행하여 제안하였고, 겉보기 동적증가계수로부터 관성효과를 보정하여 순수 변형속도 효과에 의한 동적증가계수를 제안하였다. 제안한 순수 변형속도 효과에 의한 동적증가계수의 검증을 위하여 제안한 동적증가계수 및 주요 동적증가계수를 콘크리트 SHPB 실험 유한요소해석 모델에 적용하여 검증 해석을

수행하였고, 제안한 동적증가계수를 사용할 경우 높은 정확도로 동적강도를 예측할 수 있었다.

본 연구에서 동적재료실험에서 발생하는 관성효과를 보정하기 위해 적용한 방법론은 섬유보강콘크리트 등 시멘트계 재료의 내충격성능 및 방폭성능 평가에도 활용될 수 있으며, 본 연구결과는 극단상황 하 콘크리트 구조물의 거동 예측 및 안전성 평가, 설계에 유용하게 활용될 수 있을 것으로 기대된다.

주요어: 동적증가계수, 변형속도 효과, 관성효과, 변형률 속도, 변형률 가속도, split Hopkinson pressure bar, 콘크리트 압축강도

학번: 2015-22930